JAAS

Recent advances in LIBS and XRF for the analysis of plants

Journal:	*Journal of Analytical Atomic Spectrometry*
Manuscript ID	JA-CRV-08-2017-000293.R2
Article Type:	Critical Review
Date Submitted by the Author:	19-Apr-2018
Complete List of Authors:	Arantes de Carvalho, Gabriel; Universidade de Sao Paulo, Instituto de Química Guerra, Marcelo; Black Hills State University, School of Natural Sciences Adame, Andressa; Universidade de São Paulo, Nomura, Cassiana; Instituto de Química, Universidade de São Paulo, Química Fundamental Oliveira, Pedro; University of Sao Paulo, Department of Fundamental Chemistry Pereira de Carvalho, Hudson Wallace; Universidade de Sao Paulo, Centro de Energia Nuclear na Agricultura Santos Júnior, Dário; Universidade Federal de São Paulo, Ciências Exatas e da Terra Nunes, Lidiane; Universidade de Sao Paulo Centro de Energia Nuclear na Agricultura Krug, Francisco José; Universidade de São Paulo, Centro de Energia Nuclear na Agricultura

Recent advances in LIBS and XRF for the analysis of plants

Gabriel Gustinelli Arantes de Carvalho,*[a] Marcelo Braga Bueno Guerra,[b] Andressa Adame,[c] Cassiana Seimi Nomura,[a] Pedro Vitoriano Oliveira,[a] Hudson Wallace Pereira de Carvalho,[c] Dário Santos Jr,[d] Lidiane Cristina Nunes,[c] Francisco José Krug[c]

[a] *Departamento de Química Fundamental, Instituto de Química, Universidade de São Paulo, Av. Prof. Lineu Prestes, 748, 05513-970 São Paulo, SP, Brazil*

[b] *School of Natural Sciences, Black Hills State University, 1200 University St., 57799, Spearfish, SD, USA*

[c] *Centro de Energia Nuclear na Agricultura, Universidade de São Paulo, Av. Centenário 303, 13416-000, Piracicaba, SP, Brazil*

[d] *Departamento de Ciências Exatas e da Terra, Universidade Federal de São Paulo, Rua Prof. Artur Riedel, 275, 09972-270, Diadema, SP, Brazil*

*Corresponding author:

E-mail: ggac@iq.usp.br; Tel: +55 11 3091 9104

Summary

The ability to provide a fast and multielemental analytical response directly from a solid sample makes both laser-induced breakdown spectroscopy (LIBS) and X-ray fluorescence spectrometry (XRF) very versatile tools for plant nutrition diagnosis. This review focuses on the main developments and advances in LIBS and XRF in the analysis of plant materials over the last ten years. Fundamental aspects and instrumentation are given for both techniques. The developments in the quantitative analysis of plant leaves are discussed, with special emphasis on the key aspects and challenges concerning field sampling protocols, sample preparation, and calibration strategies. Microchemical imaging applications by LIBS and XRF (including synchrotron radiation) are also presented in a broader selection of plant compartments (*e.g.*, leaves, roots, stems, and seeds). Challenges, expectations and complementarities of LIBS and XRF towards plant nutrition diagnosis are thoroughly discussed.

1 - Introduction

Macro- (C, H, O, N, P, K, Ca, Mg, S) and micronutrients (Fe, Cu, Mn, Zn, B, Mo, Cl, Ni)[1, 2] are required for healthy plant growth and can decrease crop yields if not present in appropriate mass fractions in the different plant tissues.[3-5] Additionally, beneficial elements (*e.g.*, Al, Co, Na, Se and Si) promote growth and may be essential to particular taxa, but are not required by all plant species.[2] The functions and mass fractions of these elements vary substantially among plant species.[2] For instance, Si-based fertilizers have provided considerable improvements in productivity of crops from the *Poaceae* family, such as sugar cane, maize, wheat, and rice.[6] Supplementary information on the roles of macro-, micronutrients and even beneficial elements on several crops are given elsewhere.[1, 7]

The mineral nutrition status of plants is often assessed by foliar diagnosis. By applying this strategy, plant production can be optimized by the correction of any deficiency that may limit the adequate development of *e.g.* cereals, vegetables and fruits.[3] Elemental analysis of plant tissues is an important tool not only from the agronomic point of view, but also in ecological and physiological studies.[8, 9]

For instance, the first action in agricultural management practices towards plant nutrition diagnosis is the inspection of plant leaves in the field, which may reveal characteristic visual symptoms of nutrient(s) deficiency(ies), or even toxicity. However, there are some cases where the plants do not develop deficiency symptoms when an essential nutrient is poorly available, being not possible to determine any visual difference between healthy and unhealthy plants. A less expressed deficiency (*i.e.*, a hidden

deficiency) can only be identified with the assistance of advanced spectroanalytical techniques appropriate for *in situ* plant nutrition diagnosis, such as X-ray fluorescence spectrometry (XRF), laser-induced breakdown spectroscopy (LIBS), near infrared spectroscopy (NIR), and chlorophyll (Chl) *a* fluorescence.[10] Those fast-response spectroscopy approaches offer rapid and easy-to-use means for assessing plant nutritional status; their feasibility and applicability (*i.e.*, special features, drawbacks, and validity of results) to be used either in the lab or directly in the field were recently reviewed by van Maarschalkerweerd and Husted.[10]

For plant nutrition diagnosis, the nutrients mass fractions in plant leaves are usually compared to reference values, which are commonly expressed as either sufficiency ranges (SR) or critical threshold concentrations (CTC). SR are the nutrient mass fractions at which plants are adequately nourished,[10] whereas the CTC closely match the inferior limits of the SR, and correspond to the conditions wherein plants are more likely to produce 90 percent of their maximum theoretical yields.[4] **Table 1** presents the SR of macro- and micronutrients in selected crops.

The most common approach for routine analysis of plant leaves aiming at the evaluation of their mineral content involves acid digestion followed by inductively coupled plasma optical emission spectrometry (ICP OES)[8] or inductively coupled plasma mass spectrometry (ICP-MS)[5] measurements. Modern sample preparation procedures used for plant materials are based on microwave-assisted digestion with HNO_3 + H_2O_2 in closed vessels. Nonetheless, even for these methods, sample preparation is generally the most critical step demanding much of the total analysis time. In this aspect, efforts have been made towards the direct analysis of plant materials by analytical techniques such as LIBS and XRF, among others.[3, 8]

The direct analysis of solids diminishes the number of steps in the analytical sequence and minimizes or even eliminates the generation of chemical waste.[12] In addition, other advantages have also been emphasized, such as the reduced risks of contamination and analyte losses due to the minimal sample manipulation. Furthermore, this strategy provides better laboratory safety practices and can reduce the number of uncertainty sources.[8]

In the past few years, LIBS and XRF have been experiencing a boost of applications in the extensive scenario of agricultural and environmental sciences. While LIBS has emerged in the contemporary market due to its promising features aiming at direct analysis of solid samples,[13-16] XRF has been used in several fields of applications for many decades, featuring well-established methods (including dozens of ASTM standard test methods) and commercially available instruments since the 1950s. Both techniques have been playing important roles on the recent developments in the agricultural sciences, mainly targeting at plant nutrition diagnosis.[3, 17-20]

LIBS and XRF can provide useful information on the elemental composition of solid samples, presenting attractive features such as fast analysis, high sample throughput, little or even no sample preparation, multielemental and simultaneous capabilities, non-destructiveness (particularly for XRF), and the appeal of portability.[16, 17, 19, 21-23] The possibilities to perform microchemical imaging by both LIBS and XRF provide useful information on elemental distribution within plant tissues. Recent findings have demonstrated that both techniques can be reliable alternatives to the well-established methods aiming at the determination of macro- and micronutrients in plant materials, such as ICP OES after microwave-assisted acid digestion.[17] Notwithstanding, calibration is still a

critical issue for both LIBS and XRF, which can be properly carried out when recommended boundary conditions, such as matrix-matched standards, are used.[19, 24]

This review focuses on main developments in LIBS and XRF in the analysis of plant materials over the last ten years. No attempt has been made to thoroughly quote all literature published in this period, but pioneering studies published before this period are also be considered. After introducing the fundamental aspects and instrumentation available for both techniques, this paper presents the developments in the quantitative analysis focused on the analysis of plant leaves, wherein the key aspects and challenges concerning field sampling protocols, sample preparation, and calibration, are approached. Microchemical imaging applications by LIBS and XRF (including synchrotron radiation source) are also presented in a broader selection of plant compartments (*e.g.*, leaves, roots, stems, and seeds). Challenges, expectations and complementarities of LIBS and XRF towards plant nutrition diagnosis are thoroughly discussed.

2 – Instrumentation

2.1 – Laser-induced breakdown spectroscopy

LIBS is an analytical technique that uses a laser-induced plasma as the vaporization, atomization, and excitation source to determine the elemental composition of a sample by optical emission spectrometry (OES).[13] Assorted different LIBS experimental configurations have been described in the literature.[15] The basic components of LIBS setup include: pulsed laser source(s), optical components to focus the laser energy on the sample surface and collect the radiation emitted from the excited species (*i.e.*, atoms, ions and

molecules) within the laser-induced plasma (LIP), a spectrometer coupled to a suitable detector to resolve the incoming radiation and record the emission spectra, and an electronic processing unit to synchronize the laser source and gated spectrometer.

The most used laser source applied for the analysis of plant materials is the nanosecond (ns) Q-switched Nd:YAG laser operating at the fundamental wavelength (1064 nm);[3] the second (532 nm) and fourth (266 nm) harmonics have been less employed, although benefits concerning the minimization of matrix effects and increase of measurement precision can be derived from ultraviolet (UV) laser ablation.[25] Commercially available Nd:YAG lasers present a wide pulse energy spanning range (from few mJ up to 1 J) with low shot-to-shot energy fluctuation. Femtosecond (fs) lasers can provide higher spatial resolution analysis due to lower thermal effects on sample surface and lower lateral damage after laser ablation.[26]

Plano-convex lens(es) is(are) often employed for laser focusing onto sample surface. The laser pulse energy and the optical focusing setup determine the laser fluence and irradiance on the target surface, which in turn affect the LIBS performance and detection capabilities. For a better understanding of these effects, readers are invited to read the comprehensive review from Aguilera and Aragón,[27] and specific literature concerning plant materials.[6, 23] The emitted light from the plasma is generally collected by using either plane-convex quartz lenses or mirrors, which is then focused into fibre optic cables coupled to the entrance slit of a spectrometer or directly into it. For spectral analysis and signal detection, a large variety of spectrometers is available; they are assembled *e.g.* either with *Czerny–Turner* or *Echelle* optics, and CCD (charge-coupled device) or ICCD (intensified charge-coupled device) detectors. Spectra acquisition parameters (delay time - t_d; and integration time gate - t_i) should be properly defined for appropriate time-resolved analysis.

The choice of more suitable spectrometers for plant analysis depends on the spectral selectivity and sensitivity required. For instance, spectrometers designed with *Echelle* optics and ICCD detectors offer better spectral resolution at a broad wavelength range (*e.g.*, 200 to 1000 nm) and sensitivity, being suitable for the determination of micronutrients (*e.g.*, B, Cu, Fe, Zn, Mn) at mg kg^{-1} mass fraction contents (**Table 2**).[3] On the other hand, compact spectrometers assembled with *Czerny–Turner* optics and CCD present lower performance but they are very attractive in terms of flexibility, lower cost and portability. They can be assembled as a compact multi-channel spectrometer covering a broad wavelength range (*e.g.*, from 200 to 1000 nm) with an intermediate spectral resolution (*e.g.*, 0.1 nm),[18] being suitable for portable instruments.

Besides the detector capabilities, laser fluence plays an important role on sensitivity. It has been observed that higher laser fluences (*e.g.*, 50 J cm^{-2}, at 750 μm laser spot size) increase the ablated mass, providing a larger LIP volume and higher sensitivities.[23] This is one of the main reasons that limits the performance of portable instruments equipped with relatively low-energy lasers (*e.g.*, < 50 mJ per pulse) for the determination of micronutrients in plant materials. The same is valid for fs-LIBS systems that provide smaller LIP volumes (less intense spectra) and, consequently, higher limits of detection (LOD) (**Table 2**). Of course, the development of compact high-energy lasers and high-performance spectrometers should contribute to the availability of more sensitive portable instruments in a near future. A review of the development of portable laser-induced breakdown spectroscopy and its applications is given elsewhere.[21] Typical commercial LIBS systems were compiled by Peng et al.[18]

In the last ten years, a great effort has been devoted for increasing sensitivity in LIBS, such as double-pulse LIBS (DP-LIBS), spatial-confinement LIBS, and resonance-

enhanced LIBS approaches.[18] DP-LIBS is the most commonly strategy for signal enhancement in the analysis of plant materials;[29-31] it employs a first laser pulse for ablating the sample and generating a LIP, followed by a second laser pulse (few μs interpulse delay) for re-exciting the pre-formed LIP, at collinear or orthogonal configurations.[32] For more information on DP-LIBS, readers are invited to consult the comprehensive review from Tognoni and Cristoforetti.[32] No attempt has been devoted herein to systematically discuss the LOD, which may vary substantially with the experimental setups employed. Nevertheless, the LODs from selected applications will be given in **Section 3**.

2.2 – X-ray fluorescence spectrometry

The basic XRF setup consists of a source for the excitation, optical elements to guide, shape or focus the X-ray beam on the sample and a detection system to analyse, record and register the XRF spectrum. Depending on the type of detector, features of the source, optical elements employed and the angle between them, different variants for the technique arise. In general, XRF instrumentation can be divided into two groups regarding the detection mode. The first and oldest one is the wavelength dispersive (WDXRF) detection mode and the second is the energy dispersive detection (EDXRF). WDXRF employs a crystal analyser yielding high energy resolution and sensitivity, whereas EDXRF employs detectors that are able to discriminate the energy of the X-rays that reach the detector. Energy dispersive detection is also sometimes abbreviated as EDS or EDX especially when it is coupled to scanning electron microscopes.[33]

WDXRF presents lower LODs, higher precision, accuracy and resolution in terms of differing the position and shape of transition peaks. The higher energy resolution is result of the crystal analyser that select the wavelength of the X-ray photons that will reach the

detector. This feature allows chemical speciation analysis,[34] improves the limit of detection and circumvent spectral line interferences, such as P Kα *versus* Zr Lα, Ti Kα *versus* Ba Lα, and As Kα *versus* Pb Lα.

The whole spectrum can be recorded at once by using EDXRF; in the WDXRF mode the monochromator scans through the desired narrow wavelength range. This feature makes EDXRF an ideal choice for exploratory screening. Additionally, the higher speed can be useful for high throughput systems, for samples that suffers from radiation damage, or for handheld equipment, since this detection device does not have mobile parts such as the WDXRF.

Among the X-ray-based methods, EDXRF is the most employed one for the analysis of plant materials aiming at the determination of macro- and micronutrients due to its inherent simplicity and relatively lower cost of benchtop instrumentation when compared to WDXRF. Modern high-performance benchtop EDXRF spectrometers offer several advantages, such as automated analysis, spectral deconvolution and fundamental parameter algorithms.[22] They are assembled with special chambers designed to operate under air, vacuum or helium atmosphere, being suitable for the determination of micronutrients (*e.g.*, Fe, Zn, Mn, Cu) at mg kg^{-1} mass fraction range (**Table 2**), with appropriate energy resolution.[19, 22, 35] A systematic discussion concerning the instrumentation of both WDXRF and EDXRF for the analysis of plant materials is given in the comprehensive review of Marguí et al.[19]

Only excitation by X-rays is covered herein; nevertheless the readers must keep in mind that this process can also be accomplished using particles such as electrons, positrons or ions.[36] The excitation by X-rays can be performed using radioactive sources or X-ray tubes; the latter one is far more used than the first. The X-rays generated by these tubes can

directly excite the sample; this is the most common approach in commercial equipment. However, intending to reduce the background due to X-ray scattering, the primary beam can be polarized through reflection on metallic surfaces or excite a second metallic target. Perhaps, the most important and recent innovation on X-ray tubes regards the production of the called microfocus tubes.[37] In these tubes, electromagnetic lenses focus the electron beam generated in cathode, and a smaller spot collides against the anode therefore producing a brighter X-rays beam. Additionally, XRF measurements can be carried out in synchrotron radiation facilities. These sources present higher brilliance, smaller beam size and polarized radiation, which in turn means higher sensitivity, lower LODs and higher spatial resolution than that provided by X-ray tubes.[19]

The X-ray beam can be even shaped or focused on the sample. Decreasing the beam size allows one to analyse a specific area of the sample, usually this is called micro-X-ray fluorescence spectrometry (μ-XRF). The simplest optical elements that delimit the analysed area are collimators or slits; their main drawback is the reduction of photon flux. This can be circumvented using bended mirrors, *e.g.* Kirkpatrick-Baez systems,[38] or capillaries.[39] Mono and polycapillaries are currently found in benchtop systems dedicated to microanalysis. In synchrotron beamlines one can also find microbeams produced by Fresnel zone plates.[40] In benchtop instruments, the X-ray beam size on the sample can reach tens of micrometers whereas in synchrotron beamlines spot sizes are in the range of tens of nm.[41]

Once a μ-X-ray beam is available, one can perform pinpoint analysis or carry out scans in one or two dimensions, *i.e.* line or map scans, in order to create a microchemical image; the same is possible for LIBS. A combination of two polycapillaries focusing the incoming beam on the sample and collecting the outgoing X-ray photons result in confocal

measurements, *i.e*. in this geometry one can probe specific volumes of the sample under analysis.[42]

There are several types of energy dispersive detectors; they are based on semiconductors such as lithium-doped silicon detector [Si(Li)], PIN diode or silicon drift detector (SDD). Si(Li) can be manufactured thicker than SDD detector making them more suitable for higher energies, however they need to be cooled by liquid N_2. Most of current benchtop instruments are equipped with either [Si(Li)] or SDD detectors. PIN diode is cheaper and can be produced with larger area providing larger solid angle for photon detection, whereas SDD presents higher energy resolution, *ca*. 125 eV for Mn *Kα* compared to 140 eV of Si PIN. There are also arrays of energy dispersive detectors forming a pixelated detector that allows to record chemical images without scanning the sample, such as the colour X-ray camera.[43]

The miniaturization of X-ray tubes and detectors allowed the manufacturing of reliable handheld portable XRF (P-XRF) spectrometers, which are equipped with Peltier-cooled SDD detectors and X-ray tubes with 50 kV maximum voltage. Portable vacuum pumps can enhance sensitivity for the detection of low atomic number (*Z*) elements. At the moment, P-XRF instruments present similar analytical performance to benchtop units in the analysis of plant materials.[22] Noteworthy, P-XRF also provides appropriate LOD values aiming at plant nutrition diagnosis (**Table 2**). Notwithstanding, the detection of low *Z* elements such as Si, P and S, which is limited by their low fluorescence yields, may be improved by using X-ray tube anodes made from low *Z* elements (*e.g*., Cr).[44]

3 – Quantitative analysis of plants

Substantial progress has been reached towards quantitative plant analysis by both LIBS and XRF, *i.e.*, the appropriate mathematical conversion of the emission intensities of the selected emission lines and X-ray characteristic energies, respectively, into elemental mass fractions for the corresponding analytes. Despite the use of matrix-matched standards has been recommended,[45] obtaining accurate results encompasses the strictly usage of some boundary conditions concerning *e.g.* sample presentation and instrumental conditions in order to compensate for undesirable matrix effects. In case of LIBS, these effects arise from the complex nature of laser-sample interaction, which depends on both the laser characteristics (*e.g.*, pulse duration, wavelength, fluence) and test sample properties (*e.g.*, matrix composition, particle size distribution).[14,15] In case of XRF, the X-ray absorption and enhancement, as well as physical properties of the test samples (*e.g.*, thickness, and surface uniformity), are relevant variables.[19,46]

When key requirements concerning sample presentation (*e.g.*, pellets prepared from particles < 100 μm),[45] suitable operational conditions[22,23] and calibration (*e.g.*, multivariate modelling [25,47]) are met, LIBS and EDXRF can be recommended for the quantitative determination of elemental mass fractions in plants aiming at plant nutrition diagnosis. As already mentioned, quantitative analysis can be properly carried out with calibration standards in the form of pressed pellets presenting similar physical and chemical matrix composition and known analytes mass fractions. This section highlights the most recommended boundary conditions for obtaining reliable results and presents selected contributions on quantitative analysis of plant materials by LIBS and XRF.

3.1 – Field sampling protocols

According to Roy et al.,[4] representative sampling should be done from specific plant parts at a growth stage that closely associate with the corresponding crop critical levels. Sampling criteria and the detailed procedure for individual samples collection should be representative of the field and may vary substantially in accordance to the crop under investigation. **Table 3** presents the recommended sampling protocols for plant nutrition diagnosis of selected crops, such as rice, sugar cane, citrus, maize, soybean, and wheat. Complementary information concerning the sampling protocols for other crops is given elsewhere.[11, 48]

3.2 - Sample preparation for quantitative analysis

The analysis of plant materials by XRF and LIBS encompasses some key sample preparation steps when quantitative analysis is required. In general, the direct determination of essential and beneficial elements in plant materials is carried out in leaves properly collected, and requires, at least, three sample preparation steps, namely cleaning (washing), drying and homogenization; the latter being attained after grinding and, if necessary, a further comminution step. Pelletizing is often recommended for quantitative analysis by LIBS, whereas one should also consider the possibility of analysing test samples in the form of loose powder by XRF.

As plant materials are intrinsically inhomogeneous at a microscopic scale, comminution procedures are generally mandatory for improving matrix homogenization.[45, 49] This is a critical issue especially for LIBS and μ-XRF, wherein the small mass of the test portions (*e.g.*, 0.001–10 mg) may not represent the bulk sample composition.[3, 50]

Several types of instruments can be used for plant material comminution,[49, 51, 52] including knife, ball (*e.g.* agate, tungsten carbide, stainless steel, zirconia devices),[49] cryogenic,[49] and air jet milling systems.[53] The choice of grinding method should be done in accordance with sample properties like fiber, lignin and cellulose contents,[48] and target analytes to avoid contamination from grinding devices.[52] Detailed information on grinding methods for plant materials can be found elsewhere.[49, 52]

On the other hand, when dried (unground) or *in natura* plant leaves are under investigation, a simple cleaning step (superficial washing) is recommended.[17] This issue will be described in **Section 4.1**. Also, readers must keep in mind that moisture content is a relevant variable that limits the performance of both LIBS and XRF methods (*e.g.*, shot-to-shot fluctuation in LIBS and attenuation of low energy X-ray photons), and should be corrected for.[54]

3.2.1 – LIBS

The direct analysis of powdered test samples fixed onto an adhesive tape can be regarded as a simple and straightforward strategy for LIBS analysis;[55] however, the most recommended procedure is the analysis of test samples previously pressed as pellets.[3] In the pelletizing step, the powdered laboratory sample (0.5 to 1.0 g) is transferred to a stainless steel die set being firmly pressed into a hydraulic press for obtaining a rigid pellet, with uniform surface.[3]

When aiming at quantitative results, pressed pellets should be prepared from laboratory samples presenting narrow particle size distribution with particles usually smaller than 100 μm, which is of key importance for appropriate sample presentation for analysis.[45, 49] In order to reach such requirements, either cryogenic grinding or planetary

ball milling are adequate choices.[49] For most plants,[25] this approach provides cohesive pellets, with appropriate mechanical resistance against the shock wave formed during expansion of laser-induced plasma.[45] The cohesion plays an important role on measurement precision because the more compact the pellet, the more reproducible the laser-sample interaction.[45, 56] Substantial changes in the morphology of craters formed on the surface of pellets prepared from different particle size distributions have been reported elsewhere.[3, 45]

Readers should be aware about the risks of elemental fractionation associated to sieving procedures (i.e. chemical segregation),[45] which should be carefully evaluated for each plant species.

When the ground test sample cannot be properly pelletized, a binder agent should be added for increasing the cohesiveness and mechanical resistance of the pellet, minimizing the variability between test samples.[57] Among the different binders used for pellets preparation (*e.g.*, polyvinyl alcohol, Ultrabind®, polyethylene, KBr, starch, boric acid, epoxy resin[58]), cellulose is the most recommended for the analysis of plant materials by LIBS. It is added from 10 to 50 % mass fraction, and should be thoroughly homogenized with the laboratory sample before pressing. A general overview on sample preparation aiming at LIBS analysis is given by Jantzi et al.[59]

3.2.2 – XRF

Most of the aspects concerning the sample preparation for LIBS analysis of plant materials also applies for XRF. Notwithstanding, particle size distribution is not as critical as for LIBS. Since no laser ablation takes place in XRF analysis, the requirements of mechanical resistance are less relevant. Omote et al.[60] observed that the measured X-ray intensity became constant when particles of plant material were smaller than 710 μm, and

recommended to press as pellets laboratory samples presenting particles smaller than 500 μm. Once the material is appropriately converted into a fine powder, the obtained test sample can be presented to the XRF analysis as a loose powder or after preparing a pressed pellet.[61]

At the same fashion for LIBS, the addition of a binder can be helpful for some applications. The desired characteristics of a binder are: high-purity, low X-ray absorption, and good stability under the normal operating conditions (*i.e.* vacuum and the irradiation beam).[19] Wax,[62, 63] cellulose,[64] boric acid,[65] and epoxy resin[66] are the most commonly used binding agents in the analysis of plant materials by XRF.

Alternatively, the loose powder can be simply poured into a sample holder[67] previously sealed by a thin-film, which is commercially available in different polymeric materials, such as Etnom®, Kapton®, Mylar®, Prolene®, Ultralene®, Ultra-Polyester®, Zythene®, as well as those made of polycarbonate and polypropylene.[68] The procedure is simpler and allows the re-utilization of test samples. Notwithstanding, test sample presentation in the form of pressed pellets generally offers more reproducible conditions, and the possibility to perform cross-validation between XRF and LIBS methods.[64]

3.3 - Calibration strategies

Calibration is still a challenging task when dealing with direct solid analysis. This is particularly true for matrix-dependent calibration methods such as LIBS and XRF, as well as for other techniques such as laser ablation inductively coupled plasma optical emission spectrometry / mass spectrometry,[69] especially when appropriate certified reference materials (CRMs) are not available.[24]

3.3.1 – External calibration

The flowchart in **Figure 1** summarizes the calibration strategies commonly employed in the quantitative determination of analytes mass fractions in plant materials by LIBS and XRF. For instance, external calibration using univariate methods is the first choice due to the simplicity in terms of number of calibration samples and data handling. On the other hand, better predictive ability can be derived from multivariate modelling, which attains better flexibility and robustness for such complex spectra, especially when dealing with a heterogeneous population of test samples.[25] Nonetheless, both uni- and multivariate approaches are recommended, especially when matrix-matched standards are available.[47]

Univariate linear regression models are generally built with a set of either CRMs or standards with similar matrix composition.[3, 19, 24, 70, 71] When CRMs of plant leaves are employed, the lack of commutability (*i.e.*, the low physical and chemical properties resemblance) between CRMs and test samples is often the main reason for biased results.[3, 9, 19, 72, 73] In addition, given the scarcity of commercially available CRMs of plant materials presenting elemental mass fractions spanning several orders of magnitude,[3, 70, 71] and the difficulty in finding standards with similar matrices (*e.g.*, physical and chemical properties) as for the test samples,[3, 19, 70] alternative calibration strategies have been recommended for quantitative analysis.

A feasible alternative consists in analysing a selected subset of the samples by a validated reference method, usually based on microwave-assisted acid decomposition of the powdered test samples with further analysis by ICP OES.[8, 10, 74-77] This strategy has been successfully employed for the analysis of plant materials by LIBS, such as sugar cane leaves,[6, 47] and a assorted plant species,[25, 29, 57, 72, 73]; and by EDXRF, such as coffee leaves

and branches,[78] sugarcane leaves,[8, 22] grains of rice,[67] wheat,[74] pear millet,[67] wheat flour,[64] pinna, stipe and root of ferns.[79]

A novel strategy for calibration aiming at the determination of P, K, Ca, Mg, Cu, Mn and Zn in sugar cane leaves by LIBS was proposed by Gomes et al.[24] A blank (or a low mass fraction standard) was obtained after the analytes extraction from the leaves with 0.2 mol L^{-1} HNO_3. Thereafter, a set of matrix-matched standards was prepared by mixing the raw material with the corresponding blank, at different ratios, and pressed them into pellets. This approach provided accurate results for the aforementioned elements in a set of test samples from 17 sugar cane varieties, and it was useful to extend the calibration range towards lower elemental mass fractions. It should be commented that the application of this procedure might be extended for XRF analysis (including other direct solid sampling techniques) and other plant species as well.

Care must be taken concerning the reliability of results generated by the comparative method, because any difference observed between the reference laboratory data and the analytical response will be necessarily due to one or more of the following factors: instrument errors, reference data errors, or the lack of correlation between them. In the case of XRF and LIBS, the instrument and the lack-of-fit errors tend to be minimal when optimized operating conditions are selected. Then, the total error will be almost entirely due to the comparative method. This issue was addressed by Souza et al.[6] when searching for a reliable comparative method for silicon determination in sugar cane leaves. According to these authors, obtaining accurate results by the reference method was decisive for attaining trueness of LIBS calibration. However, according to Mark,[80] one must be aware that the reliability of calibration is also affected by a chain of interrelated conditions, such as: (i) the range of the analyte mass fractions and their distribution within the range;

(ii) the number of calibration samples; (iii) the sample preparation method; (iv) selection of samples for the calibration set; and (v) the interpretation of the calibration model and data handling. Additionally, the commutability must be assured when CRMs are chosen for building the calibration models, which means that the measurement behaviour between the CRMs and test samples are mathematically equivalent.[81, 82]

Another widespread calibration approach in XRF is based upon the preparation of a set of synthetic standards by spiking cellulose powder with increasing amounts of the analytes.[9, 70, 83] Robinson et al.[83] employed this strategy for the determination of sulphur in biomass feedstocks by EDXRF. A calibration set from 2 to 2250 mg kg^{-1} S was obtained from the analyte addition to microcrystalline cellulose reaching a limit of detection of 2 mg kg^{-1} S. Notwithstanding, this procedure has not been recommended for LIBS due to the high dependence of matrix properties on calibration.

Multivariate calibration methods such as partial least squares (PLS) regression have been used for quantitative analysis of plant materials.[25, 47, 57] These advanced methods are more compatible with the spectra complexity, especially for LIBS, as factors related to variations in the analytical response can be efficiently regressed against the properties of interest.[3] For building multivariate regression models, the spectral regions, the preprocessing methods, and the number of PLS factors should be optimized for each analyte.[25] Ideally, each factor added to the calibration model would describe the variation, which is relevant for predicting property values.[84] Particularly for LIBS, when a high number of emission lines is available for an analyte, interval PLS regression can be used for the selection of the best spectral region, as demonstrated elsewhere.[47, 57] Spectral preprocessing (*e.g.*, constant offset elimination, vector normalization) can deliver to the PLS models not only an improvement in its prediction ability but also a greater flexibility

for fitting.[25] These normalization procedures can be exploited for correcting matrix effects, fluctuations and instrumental drifts.[85] The theoretical basis of the PLS algorithm is given elsewhere.[57, 86]

Supervised multivariate classification approaches such as principal component analysis (PCA)[47] and hierarchical cluster analysis (HCA)[25] are useful for evaluating classes among test samples in order to select representative calibration and validation sets for designing and testing the multivariate prediction models. These methods are also useful for the identification of outliers prior to the multivariate calibrations. Alternative approaches for outliers identification are described elsewhere.[87, 88] Statistical parameters such as the correlation coefficients of calibration models and the root mean square error of calibration should be employed to evaluate the quality of the models such as the coherency of the univariate and multivariate fittings. The prediction ability of the calibration models is often evaluated using the root mean square error of prediction, the coefficient of regression of validation samples, the quality coefficient, and the residual predictive deviation parameters, among others.[87]

PLS models have been successfully used in the analysis of plant leaves.[25, 57, 47, 89] Awasthi et al.[90] demonstrated that multivariate-based models such as PLS regression and PLS discriminant analysis (PLS-DA) provided accurate results for Al, Ca, Fe, K and Mg in different CRMs using LIBS. Although it has not been well exploited up to the moment, multivariate modelling can be also recommended for XRF, especially for EDXRF that presents lower spectral resolution.

For instance, internal standardization can correct for random fluctuations of the emission intensities by normalizing the analytical response of the analyte by the corresponding one from an internal standard.[57, 91, 92] Carbon emission lines (C I 193.090

and C I 247.856 nm) have been used as internal standards in the analysis of plant materials by LIBS.[57, 92, 93] Notwithstanding, the possibilities of potential interference on C I 247.856 nm caused by Fe emission lines should be considered. Normalization of analytes emission lines by the emission background has been also proposed for the analysis of plant materials by LIBS.[75] Of course, by taking into account the well-known advantages of internal standardization in other atomic spectrometric techniques, this issue should be better explored in LIBS and XRF. According to Marguí et al.,[19] internal standardization is not commonly used in XRF analysis of plant materials.

3.3.2 – Standardless calibration

Standardless calibration strategies have been approached for XRF [Fundamental parameters (FP) and Emission-transmission methods] and LIBS (Calibration free method; CF-LIBS).

The FP method, which was originally proposed in 1955,[94] is also available for analysis of plant materials by XRF.[60] This method is based on X-ray physics parameters, which enables the formulation of a mathematical algorithm that theoretically correlates the characteristic X-ray emission intensities and the elemental mass fractions of the test sample.[95] A detailed description of the mathematical basis of the FP method can be found elsewhere.[95]

Shaltout et al.[96] employed the fundamental parameters method for the quantitative determination of P, K, Ca, Mg, S, Fe, Cu, Mn, Zn, Al, Br, Cl, Na, Ni, Rb, Si, Sr, and Ti in leaves and stalks from a medicinal plant by WDXRF. Test samples were prepared after washing, oven drying at 70 ºC, sieving through a 32 μm sieve, and a pelletizing step. A CRM of green tea was used for checking the trueness of the method.

Several XRF instruments are sold with pre-calibrated methods for different matrices; however, no guarantee related to the accuracy is provided by the manufacturers.[97] In this regard, Andersen et al.[97] evaluated the performance of a commercial pre-calibrated/standardless method commercialized with a WDXRF spectrometer. Thirteen CRMs of plant materials were analysed allowing the detection of P, K, Ca, Mg, S, Fe, Cu, Mn, Zn, Mo, Ni, Cl, Al, As, Ba, Cr, Na, Pb, Rb, Sr, and V. Relative errors below 20 % to better than 10 %, depending on the elemental mass fractions, and measurement precision lower than 5 % (for detected levels higher than 25 mg kg^{-1}), were typically observed. Nevertheless, some elements experienced anomalous relative biases (as high as 40 %), which advises the analyst for the validation of the method.

The emission-transmission (ET) method is another standardless option for XRF quantitative analysis, which was originally proposed by Leroux and Mahmud in 1966.[98] It is based on the measurement of the X-ray radiation from the test sample alone, the test sample and a solid target positioned just behind it, and only the target.[46, 99] The ET method is a particularly interesting choice, because it can circumvent the matrix effects;[100] however, the test samples must present intermediate thickness. Blonski et al.[35] used the emission-transmission calibration strategy for the determination of the chemical composition of citrus leaves. An EDXRF method was evaluated to investigate the effects of the fumagina disease on the mineral profile of samples by comparing the Ca, Ti, Mn, Fe, Cu, and Zn mass fractions of healthy and infected orange and lemon leaves.

CF-LIBS is an approach to multi-elemental quantitative analysis which does not require the use of calibration curves and/or matrix matched standards.[101] In CF-LIBS, an algorithm based on the measurement of line intensities and plasma properties (plasma electron density and temperature), on the assumption of a Boltzmann population of excited

levels, is used to determine elemental mass fractions. This method has been evaluated for the determination of Ca, Fe, N and P in poplar tree leaves, but there is no information regarding method validation.[102] However, the performance of CF-LIBS is limited by the uncertainties of results for the major components, which reflect into a high relative error affecting the minor components.[101]

3.3.3 – Limits of detection

Table 2 presents LOD values for macro- and micronutrients for different configuration of LIBS (ns- and fs-LIBS setups assembled with ICCD detectors) and EDXRF (benchtop units and portable system assembled with Si(Li) and SDD detectors, respectively; all instruments equipped with Rh X-ray tubes). These data were derived from univariate calibration models built with the same set of sugar cane leaves (*Saccharum officinarum* L.) in the form of pressed pellets. With some few exceptions (*e.g.*, Mn in EDXRF and fs-LIBS), the LODs of both techniques are appropriate for plant nutrition diagnosis by taking into account the sufficiency ranges of nutrients in selected crops (**Table 1**). Although these LODs were determined for pellets of sugar cane leaves, they are representative values for the aforementioned LIBS and XRF configurations, and can be properly considered for other crops. In addition, a broader collection of LOD values obtained by different LIBS and XRF instruments in a great variety of applications are given in **Tables 4** and **5**.

3.3.4 - Additional remarks

LIBS and XRF techniques can provide complementary information on the elemental analysis of plant materials, as described elsewhere.[17, 64] The non-destructive

capability of XRF, the fast measurements of LIBS, and the appropriate limits of detection of both methods are appealing attributes fostering the combination of both techniques for the routine analysis of plant materials towards plant nutrition diagnosis.[17, 64]

The ability to perform cross-validation[17,46] for elements that can be commonly determined by both techniques (*e.g.*, P, K, Ca, Fe, Mn and Si) in the same test sample is a key feature in the development and validation of quantitative methods. This approach may improve the quality and reliability of the results. Noteworthy, for appropriate data comparison, equivalent sampling strategies should be considered, since there are substantial differences between the analysed area in LIBS (*e.g.*, 100-1000 μm spot diameter) and XRF (*e.g.*, 1-5 mm spot diameter).

3.4 – Selected applications

3.4.1 - LIBS

The improvement in instrumental capabilities and knowledge on fundamental aspects of laser-induced plasmas have boosted a large expansion into laboratory applications. As a result, LIBS is now competing with other conventional laboratory techniques, mainly for solid sample analysis.[3, 18, 103, 104] According to Hahn and Omenetto,[14] quantitative analysis is still an issue for LIBS and it has been considered the *Achilles heel* of this technique. The complex nature of laser-sample interaction, causing strong and undesirable matrix interferences, and the plasma-particle interactions processes are the main challenges to be overcome.[15] The use of adequate calibration strategy associated to the optimization of instrumental parameters (*e.g.*, laser fluence, wavelength, pulse

duration), and the adequate presentation of test samples (*i.e.*, pellets prepared from particles < 100 μm), are some important steps to obtain reliable data in the quantitative analysis.[25]

Recently, Peng et al.[18] have drawn attention to key aspects towards consolidation of LIBS as a reliable technique for the analysis of agricultural samples, such as: (i) the use of chemometrics for improving performance of calibration and classification; (ii) integration of LIBS data with those from others analytical techniques, such as Raman spectroscopy or NIR spectroscopy (data fusion approach); (iii) development of more compact and reliable fieldable instruments; and (iv) better understanding of the mechanisms underlying the laser-sample interaction.

Variations in emission signal intensities as a function of particle size are one of the main reasons for biased results. The incomplete decomposition of larger particles increases the number of atoms in the laser-induced plasma that remain in a non-emitting phase bound within the solid particulate, resulting in lower emission signal intensities.[45, 105] This aspect was investigated for pellets of sieved plant materials (passed through 150, 106, 75, 53 and 20 μm sieve apertures), wherein it was demonstrated that matrix effects were minimized, or even eliminated, when pellets were prepared from particles smaller than 100 μm.[45] In addition to the similarity of the chemical matrix, close resemblance between particle size distribution of standards and test samples is also recommended.

One must also consider that the physical processes involved in laser-sample interaction, as well as in dynamic expansion of plasma, are dependent on the matrix composition and experimental conditions, such as laser wavelength, fluence, spot size, and plasma volume.[23, 45, 105] The choice of appropriate laser fluence (*i.e.*, 50 J cm^{-2}, Nd:YAG@1064 nm) can overcome variations within test sample properties,[45] and was

decisive for obtaining accurate measurements of Ca, K, Mg, P, Al, B, Cu, Fe, Mn, Zn [23] and Si [6] in the analysis of pellets of sugar cane leaves from 23 varieties.

A systematic comparison between analytical performance of a nanosecond (6 ns Nd:YAG laser at 1064, 532 and 266 nm) and femtosecond (60 fs Ti:Sapphire at 880 nm) LIBS systems was carried out for the analysis of a heterogeneous set of samples, composed by pellets from 31 plant species.[25] HCA was performed to select representative calibration (n_{cal} = 17) and validation (n_{val} = 14) datasets. Predictive functions based on univariate and multivariate modelling of optical emissions associated to macro- (Ca, Mg, and P) and micronutrients (Cu, Fe, Mn and Zn) were built. fs-LIBS provided accurate results on the determination of analytes mass fractions, whatever the modelling approach. Although predicted values by ns-LIBS multivariate modelling exhibit better agreement with reference mass fractions as compared to univariate functions, fs-LIBS conducts better quantification of nutrients in plant materials since it is less dependent on the chemical composition of the matrices.

A protocol for the quantitative direct analysis of dried leaves was proposed by Guerra et al.[17] The proposed sampling protocol (**Figure 2**) relied on the rastering of 3 equally spaced sampling lines in each leaf fragment (9 mm x 9 mm area) with 48 accumulated laser pulses *per* line (Nd:YAG at 1064 nm, 5 ns, 10 Hz, 50 J cm^{-2}) perpendicular to the leaf midrib. This strategy enabled the simultaneous determination of P, K, Ca, Mg, Fe, Cu, Mn, Zn, B and Si by LIBS. Cross-validation between LIBS and EDXRF for P, K, Ca, Fe, Mn and Si predicted mass fractions presented high linear correlation coefficients of up to 0.9778 (selecting 15 leaf fragments *per* diagnostic leaf from 10 different sugar cane varieties). According to the authors, the results provided insights into a novel and promising strategy for direct and fast plant nutrition diagnosis,

fostering further studies for *in situ* analysis of fresh leaves, strengthening the implementation of Precision Agriculture and Green Chemistry concepts.

Recently, Jull et al.[106] evaluated the feasibility of LIBS for the analysis of fresh pasture (ryegrass and clover leaves) samples. PLS regression was used to build models for macro- (N, P, K, S, Ca and Mg), micronutrients (Fe, Mn, Zn, Cu and B) and Na. Authors highlighted some key aspects that limit obtaining accurate results in the *in situ* analysis of fresh leaves when comparing to the analysis of dried test samples (*i.e.*, pellet), such as the ablation atmosphere and the moisture content. The latter one varied substantially between fresh test samples and affected emission lines intensities, since the higher the moisture level, the weaker the emission spectra intensity. Although the predictive abilities of calibration models designed for fresh leaves have been inferior to those created for pellets, they were appropriate for semi-quantitative analysis (*i.e.*, estimation of nutrient levels), being able to identify whether nutrient levels are within a certain range or not. These findings are relevant for real time decision making on the type of fertilizer needed in specific areas of a field. According to the authors, the implementation of an *in situ* LIBS instrument would require some technical progresses towards an autofocus system to mitigate the variabilities caused by lens-to-sample distance, and mechanical assemblies to reduce vibrations, for example.

Table 4 summarizes selected applications of LIBS analysis of plant leaves published in the last 10 years. Additional contributions regarding other plant tissues are given in the comprehensive review from Santos Jr. et al.[3]

3.4.2 - XRF

X-Ray fluorescence spectrometry (XRF) has been widely regarded as a powerful analytical tool in plant nutrition diagnosis.[10, 19, 70, 110] Its non-destructive,[60] simultaneous and multielemental capabilities[19] combined with the simple sample preparation steps [60, 70] have paved the way towards its adoption in several routine analytical laboratories.[20]

Marguí et al.[70] employed a WDXRF instrument for the quantitative determination of macronutrients (P, K, Ca, Mg, S), micronutrients (Mn, Fe, Zn) and non-essential elements (As, Al, Co, Na, Sr, Pb) in pellets of plant materials. According to the authors, the combination of plant CRMs and synthetic standards made of cellulose spiked with appropriate amounts of analytes was effective for obtaining calibration curves that predicted reliable results. In another contribution, the same research group [76] obtained accurate results by EDXRF in the analysis of leaves of higher plants cultivated in a contaminated area. The CRM orchard leaves (NIST SRM 1571) was used for accuracy evaluation, and the results for K, Ca, Mn, Fe, Cu, Sr, Pb and Zn were in good agreement with the corresponding certified mass fractions.

Portability is an appealing attribute offered by XRF analysis. In this sense, several recent studies have demonstrated the analytical performance of portable XRF (PXRF) spectrometers in the analysis of vegetation,[9, 22, 77, 110, 111] PXRF (handheld) systems are a cost-effective and an option for those who intend to carry out faster *in situ* and laboratory analysis with equivalent performance of the benchtop units.[22]

Mclaren et al.[111] described pioneering investigations demonstrating the feasibility of PXRF systems in plant nutrition diagnosis. Samples from important crops (*i.e.*, corn, cotton, soybean and wheat) were analysed by the loose powder method with measurement times varying from 120 to 420 s. Linear correlations were observed between reference mass

fraction data obtained by a validated ICP OES method and the X-ray emission intensities from P, K, Ca, S, Fe, Mn, Zn, Co, Cr, Ni, and Si.

Reidinger et al.[9] also evaluated a PXRF system for the determination of Si and P in pellets prepared from ground leaves of plants from the *Poaceae* family. The calibration approach was based on the preparation of standards of spiked methyl cellulose as a way to simulate the plant matrix. Calibration curves from 2.5 to 10 g kg^{-1} P and from 5 to 100 g kg^{-1} Si were successfully obtained from measurements carried out under helium atmosphere to avoid the attenuation of the low-energy P and Si photons by the air. The estimated detection limits were similar for both analytes: 0.13 and 0.14 g kg^{-1} for P and Si, respectively. High accuracy and analytical throughput, enabling processing up to 200 test samples a day, as well as the small amount of sample required for analysis in a non-destructive way, were pointed as outstanding benefits of the proposed method. In addition, the authors highlighted other advantages of the PXRF spectrometers such as their lower purchasing prices with the possibility to perform *in vitro* and *in situ* studies.

A systematic comparison between analytical performance of a benchtop and a handheld PXRF system was carried out by Guerra et al.[22] They reported quantitative data for P, K, Ca, S, Fe, Mn, and Si from the analysis of pressed pellets of previously ground sugar cane leaves from 23 varieties. The similar analytical figures of merit of both instruments reinforced the suitability of PXRF equipment in plant tissue analysis, especially for future promising studies related to its application for *in situ* and real time plant nutrition diagnosis.

Table 5 summarizes the sample preparation and calibration strategies employed in selected applications of XRF in the analysis of plant leaves.

3.4.3 - *In situ* foliar diagnosis

There are few attempts towards the *in situ* foliar diagnosis by using handheld P-XRF spectrometers. To the best of the authors' knowledge, Dao[122] was the first to contribute in this emerging research topic. In this study, fresh corn leaves were directly analysed in the field, and linear correlations between P Kα emission line intensities (after normalization by the Ag Lα scattered line) and the elemental mass fractions were obtained. The evaluated normalization strategy was effective for improving accuracy because it corrected for the variations in leaf composition related to the different moisture contents. The author qualified this novel spectroscopic method as a "new paradigm in nutrient management" given its outstanding features, namely non-destructiveness and high speed of analysis.

Dao[122] provided another important contribution on the use of P-XRF for the direct analysis of fresh corn leaves from phosphorus-amended soils. In this study, the uppermost leaves of plants were directly analysed by P-XRF under helium atmosphere. Some of the XRF measurements were performed *in situ* in selected plants on the 22nd, 31st, and 43rd day after planting (DAP), while they were in the ground. For the remaining samples (DAP 16, 18, 25, 39, and 51), plants were harvested and scanned at fresh conditions, and after oven-drying. Leaves from plants at similar phenological stages were also harvested for the determination of moisture content. The author raised an important conclusion from this study: "*X-ray fluorescence methods may alleviate the technological shortcomings and information gaps about inorganic macronutrients status in plant and soil. These proximal sensing methods can provide greater density of compositional measurements, and timeliness of the analytical information for precision nutrient management to fulfill some of the critical knowledge gaps. Spectral scanning of plant canopy under field conditions*

yielded multi-element concentration profiles almost instantaneously. Knowing in real time and being able to respond rapidly to changes in P availability and variable plant needs during a growing season can enhance plant productivity, farming profitability by matching nutrient inputs to actual levels needed by the crop, while minimizing agricultural impact on the surrounding environment."

More recently, Guerra et al.[123] investigated the suitability of a handheld P-XRF for real time foliar diagnosis. They proposed a sampling protocol for sugar cane crop involving the direct *in situ* analysis of fresh leaf fragments (n = 20 *per* diagnostic leaf). Calibration models for K, Ca, S, and Si were built from the analysis of a set of pellets of sugar cane leaves from 23 varieties, whose elemental mass fractions were previously determined by ICP OES after microwave-assisted acid digestion. The proposed method can be regarded as a promising tool for fast plant mineral analysis, especially when looking at the obtained LODs, which were at least two-fold lower than the recommended critical nutrient levels.

4 – Microchemical imaging: space-resolved analysis of plant tissues

The most commonly employed chemical imaging methods are those coupled to scanning and transmission electron microscopes. The main advantage of these systems consists in the high spatial resolution (*e.g.*, nanometer range) offered by the electron beam and the detection of elements with $Z < 11$.[33] On the other hand, μ-XRF offers lower detection limits for $Z > 11$, the usage of vacuum is not mandatory, and sample preparation is much simpler. One of the crucial difference between these two chemical imaging

approaches resides on the probed depth. Due to the interaction with matter, electron beams are more surface sensitive than X-rays.[33]

The development of microanalytical probes allows accessing the spatial distribution of mineral nutrients along a nonhomogeneous plant tissue, for example. Therefore, microsampling may not be representative of the whole tissue composition.[17] Nevertheless, the information obtained with these tools allows accurately assigning tissues, or structures, responsible for either translocation or storage of nutrients. Thus, microanalytical techniques have assisted in the establishment of structure-function relationships in plants. According to Wu and Becker,[124] revealing the uptake, translocation, storage and speciation of both essential and toxic elements in plants is important for understanding plant homeostasis and metabolism, providing insights into food and nutrient studies, agriculture activities and environmental sciences.

Although LA-ICP-MS has been in the forefront of chemical imaging applications in biological materials,[125, 126] due to its attractive features such as multielemental and isotopic analysis, excellent limits of detection and good resolution, no attempt has been devoted to this technique in this review.

4.1 – Sample preparation for microchemical imaging

Ideally, biological phenomena or features of plant leaves should be studied *in vivo* while they are taking place. Nevertheless, in most cases this is not feasible, and the choice of the sample preparation method is a compromise among several factors, including the imaging approach desired (*e.g.* μ-XRF 2D mapping, μ-XRF tomography or LIBS mapping). The lateral or spatial resolution may require samples sliced in thin layers. The type of X-ray source, for example, synchrotrons are much brighter than anodes and

therefore samples may have to be frozen during measurements to avoid burning or radiation damage. Hence, sample preparation in chemical imaging seeks to preserve the sample for future analysis, avoids elemental redistribution and matches the sample features, such as thickness and size, to the lateral or spatial resolution provided by the imaging technique.[127, 128]

The procedures are nearly the same as those employed in electron microscopy; the most common methods are chemical fixation and cryofixation. Additionally, in μ-XRF and LIBS imaging techniques, samples can be analysed in pristine form or *in vivo* conditions without sample preparation. In the case of LIBS, it is essential the preparation of test samples presenting flat surfaces to ensure reproducible laser ablation conditions; although ablation chambers assembled with laser auto-focus may overcome this issue. **Table 6** presents assorted sample preparation strategies that have been employed in the analysis of several plant compartments (*e.g.*, leaves, roots, stems) by μ-XRF.

The chemical fixation is a process that keeps the tissue structure and avoids putrefaction. It is achieved by the creation of chemical bonds that connect the macromolecules and therefore maintaining the tissue architecture. The most common fixative chemical groups are aldehydes, alcohols, and oxidizing agents such as osmium tetroxide.[127, 151-153] Besides preservation, chemical fixation also enhances the mechanical properties of the tissues, thus facilitating the cutting. One of the main risks involved is related to the alteration of the elemental distribution due to the possible leaching of weakly bound elements by the fixative solution. This can be critical in chemical imaging at cellular level.

Cryofixation consists in a rapid freezing of the sample to temperatures in the order of magnitude of liquid nitrogen. The flash freezing process solidifies the water and therefore

prevents the molecular and ionic transportation.[154] Metabolic reactions cease, tissue structures are preserved, and the mechanical properties of the sample are strengthened allowing it to be properly sliced. Cryofixation can be performed by plunging the sample and cryogen or through high pressure freezing.[155] The latter procedure requires special apparatus and is not as common as the immersion cryofixation and therefore it will not be addressed here. In immersion cryofixation, the tissue can be dipped and frozen directly into liquid N_2 or supercooled isopentane. Another strategy consists in firstly embedding the sample into a resin, such as optimal cut resin or acrylate, and then rapid freeze it in the liquids above mentioned. Once the sample is frozen, it can be stored in liquid N_2 until analysis.

However, Mishra et al.[156] showed that freezing the sample directly in liquid N_2 changed the spatial distribution of As at micrometric level. It happened because liquid N_2 boils when the sample is immersed into it, thus the heat transfer from the sample to the cryogen is not fast enough to prevent the formation of ice crystals. These crystals can damage the membranes and allow the migration of elements between cell compartments. To circumvent this issue, the cryofixation by immersion should be performed with nonvolatile liquids such as isopentane.

Once the sample is cryofixed, it can be sectioned in a cryostate; the procedure is called cryosectioning. Alternatively, the frozen water can be replaced by acetone [155] or sublimated through lyophilization.[157] Finally, the cryofixed sample can be embedded into resin to facilitate the slicing or be analysed as it is.

4.2 – Microchemical imaging by X-ray fluorescence spectrometry

Most of the elemental mapping studies of vegetal tissues by μ-XRF aims to elucidate the mechanisms that control the distribution patterns within hyperaccumulating plants.[79, 129, 133] The term "hyperaccumulators"[158, 159] was proposed to refer to plants that are able to handle high levels of potentially toxic elements (*e.g.*, As, Cd, Mn, Ni, Se, and Zn)[160] inside their tissues, reaching more than 1000 μg g^{-1} on a dry-weight basis. These peculiar organisms have been used in clean-up initiatives aiming at removing contaminants from the soil, as well as in other applications, such as those where they can be harvested for exploiting valuable metals from the environment.[161] X-Ray Absorption Spectroscopy (XAS) can perform chemical speciation analysis along with the elemental mapping by μ-XRF. This approach provides crucial information for designing and optimizing both phytoremediation [162, 163] and phytomining [164-166] studies with these vegetal species.[167-169] A detailed review about the available X-ray elemental mapping methods for investigating ecophysiological processes in hyperaccumulating plants was recently prepared by van der Ent et al.[170] In this study, the advantages and limitations of the X-ray methods applied to reveal the metal(loid) homeostasis in plants was critically compared.

Campos et al.[79] investigated the spatial distribution of As and P in an As-hyperaccumulator fern, *Pityrogramma calomelanos*, using a benchtop μ-EDXRF. Ferns were hydroponically grown without and with 1.0, 10 or 30 x 10^{-3} mol L^{-1} As during three weeks. The microchemical maps revealed that As was preferentially accumulated in the pinna midrib, secondary veins, apical and marginal regions of the pinnule of the fern. The high levels of As in the plant tissues led to drastic alterations in the P distribution. **Figure 3** clearly shows the antagonistic behavior of both elements since the higher levels of As in the apical portions of the pinna caused a noticeable decay of the P content in this area. Chemical imaging of biological samples by μ-XRF is a challenging task, especially when

dealing with intermediate-thickness specimens.[19] To overcome this drawback, a correction strategy based on the scattered radiation method[19] was successfully used for As taking into account the Rh Kα Compton peak. Surowka et al.[171] recently addressed the necessity of correcting matrix effects in order to obtain accurate quantitative imaging of biological tissues by XRF. The authors also reinforced that the use of Compton intensities is an appealing strategy for the quantitative imaging of heterogeneous thin-sections of biological test samples.

Punshon et al.[172] reviewed the literature on the applications in the plant sciences of micro X-Ray Fluorescence Spectrometry with Synchrotron radiation source (μ-SRXRF). They highlighted μ-SRXRF as a convenient method for the high spatial resolution mapping of *in vivo* specimens avoiding tedious sample preparation steps involving fixation, coating, drying or even cutting. Vijayan et al.[173] also emphasized the attractive features of synchrotron radiation, *i.e.* its brightness, polarization and pulse properties. Notwithstanding, they pointed out that synchrotron-based analytical methods are still underused in plant science applications. On the other hand, Wu and Becker,[124] reviewed the analytical techniques (SIMS, LA-ICP-MS, SRXRF, and XAS) applied in the chemical imaging and speciation studies in plant materials, emphasizing some limitations of synchrotron-based methods, such as: i) damaged derived from the interaction of X-rays with biological materials, and ii) restricted access to beamline time for conducting experiments. Most recently, Zhao et al.[174] reviewed the advantages and limitations of the analytical techniques available for the microchemical mapping of plant tissues. Regarding SRXRF, a promising future could be foreseen with probes capable of reaching below 100 nm resolution for the chemical investigation at a subcellular level.

A novel and ever-increasing area of study of μ-XRF mapping is presently dedicated to the investigation of the accumulation and biotransformation pathways of engineered nanomaterials (ENMs) inside plant tissues.[128] This current trend is clearly correlated with the increased utilization of ENMs in a myriad of applications in the modern society including, but not limited to, cosmetics,[175] medicine,[176] food packing,[177] and agriculture,[178] which inadvertently cause contamination to the environment.[128, 137] Hernandez-Viezcas et al.[137] evaluated the distribution patterns and the chemical forms of Zn and Ce by μ-SRXRF and μ-XANES in soybean tissues from plants grown in soils treated with ZnO and CeO_2 nanoparticles (NPs) at mass fraction levels of 500 and 1000 mg kg^{-1}, respectively. They observed that most of the CeO_2 NPs remained unchanged within the plant tissues owing to the small percentage of biotransformed Ce (III) species as revealed by μ-XANES data. On the other hand, they reported that the Zn species were not present in the form of ZnO NPs inside the plant tissues. A recent and comprehensive review made by Castillo-Michel et al.[128] provided some promising perspectives on the use of synchrotron techniques in the investigation of the ENMs fate in plants. According to the authors, this active research area can be highly benefited by the advances observed in the new generation of SR sources, which can offer outstanding analytical figures of merit, such as better spatial resolution, down to the nanometer range, lower detection limits and higher analytical throughput.

Few studies have explored the synergy between chemometrics and the wealth of information obtained from the maps of vegetal tissues by μ-XRF. Verbi Pereira and Milori [179] analysed leaves from healthy and infected orange trees with citrus greening (citrus Huanglongbing), a disease presenting a long asymptomatic period that impairs the citrus crop production. The combination of the μ-SRXRF maps and chemometric tools (PCA, SIMCA, KNN, and PLS-DA) allowed the correct classification of up to 98 % of the

samples. The most important spectral regions that enabled appropriate classification were related to the signals of K, Ca, Fe, Cu and Zn and the coherent and incoherent scatterings.

Table 6 presents an overview of recent studies focused on the μ-XRF mapping of plant tissues emphasizing the analytes under scrutiny, as well as the instrumentation used, sample preparation strategies, and the main objectives of the investigation.

4.3 – Microchemical imaging by laser-induced breakdown spectroscopy

High lateral resolution, down to few micrometers, combined with its capacity to assess the elemental profile of specimens in a fast and reproducible way are special attributes of this chemical imaging technique.[180, 181] LIBS gives an instantaneous signal directly related to the location at which a single ablation event occurred.[103] Notwithstanding, the number of application of LIBS for chemical imaging of plant tissues is limited by the relatively low sensitivities for the micronutrients at a high-resolution experimental setup. It is expected DP-LIBS approach may improve sensitivity and extend the number of chemical imaging applications.

According to Kaiser et al.,[103] resolution in chemical imaging by LIBS can be defined as the smallest distance between two ablation spots on which any potential changes in composition can be registered at a certain level of significance. Besides, the test sample properties (*e.g.*, hardness, flatness), the lateral and profile resolutions are affected mainly by the laser properties, such as the spot size on the sample surface, the pulse energy and its duration. It should be also noticed that LIBS analytical outcomes may be influenced by the re-deposition of particles from surrounding ablated craters on the fresh surface, if no buffer gas flow is used. In general terms, using low-energy (few mJ), short wavelength (*i.e.*, UV) or ultrashort duration (ps, fs) laser pulses, ablation craters with micron-scale sizes laterally

and nm scale sizes in depth can be produced.[103, 182] One should keep in mind that analytical sensitivity decreases as resolution increases; the production of smaller craters led to the vaporization of a lower amount of ablated particles within the laser-induced plasma.[103]

Femtosecond laser ablation can provide nanometer-range spatial resolution, either laterally or in depth,[183, 184] being the most recommended approach for high-resolution chemical imaging by LIBS[185] and LA-ICP-MS.[186] The ability of fs laser pulses to couple energy into material faster than energy dissipation such as heat diffusion or shock waves, enables laser ablation with less collateral damages than longer pulses,[187] being able to produce craters without high rims and other irregularities (*e.g.*, droplets), which are usually observed for nanosecond laser ablation.[188] This unique feature allows the determination of depth profiling of multi-layer samples,[185] as well as the analysis of individual plant cells.[26] Nonetheless, there are few applications in the spatial analysis of plant materials by fs-LIBS,[26, 189-191] which may be attributed to poor sensitivity achieved by these systems and high cost of instrumentation.

Several research groups have adopted LIBS as a probe for mapping plant materials. For instance, the Kaiser's group, from Czech Republic, has been in the forefront of applications[30, 103, 192-197] in this ever-expanding research field. In the same way for μ-XRF mapping, most of the studies concerning with the use of LIBS are focused on the mapping of hyperaccumulating plants. Sunflower is the target vegetal species in several studies [193-197] where LIBS was the chosen tool for mapping potentially toxic elements. Krystofova *et al.*[197] investigated the spatial distribution of Mg and Pb in leaves of maize, sunflower and lettuce, which were exposed to 0.5 or 1.0 x 10^{-3} mol L^{-1} Pb-EDTA in laboratory conditions from 3 to 5 days. The obtained results were in a good agreement with LA-ICP-MS data. In another study, Pb accumulation patterns were also revealed by LIBS in sunflower leaves

from plants grown in a lead acetate solution. Authors found that the high Pb levels inside plant tissues affected K and Mn uptake rates and their distribution profiles along the leaves compartments.

The evaluation of the accumulation pattern of engineered nanomaterials (ENMs) along vegetation tissues by LIBS is still a poorly explored research field. Most recently, Krajcarová *et al.*[30] compared the Ag spatial distribution in root cross-sections of *Vicia faba* grown in $AgNO_3$ medium or in a solution of silver NPs. A double pulse LIBS configuration was used for analyzing the root test samples previously cut into 40 μm thickness cross sections. The results shed light on the different uptake behaviours regarding the absorption profile of Ag^+ ions and AgNPs into the root tissues of the evaluated plant species, indicating that AgNPs are absorbed in a much lower rate than the ions.

LIBS can also offer the possibility of performing tridimensional mapping without laborious sample preparation steps.[181, 198] This is particularly relevant when analysing biological materials, which present inherent heterogeneous elemental distribution and are very prone to contamination. Zhao *et al.*[199] exploited this versatility by moving a LIBS system to a maize field (**Figure 4**) and performed the pioneering study involving both *in situ* and *in vivo* 3-D elemental mapping. They sprayed an organophosphorus pesticide (chlorpyrifos, $C_9H_{11}Cl_3NO_3PS$) on a maize leaf, and analysed the vegetal tissue after 10 h exposure. Pesticide residues were accurately measured after construction of multivariate regression models, where samples with known amounts of pesticide composed the calibration set, and selected P and Cl emission lines were employed as response variables. The obtained maps (12-μm step in the z-axis) clearly demonstrated that the amount of pesticide residues significantly decreased along the leaf depth and negligible levels were

detected from the fifth layer. The simplicity of LIBS systems makes this technique very promising aiming at *in situ* analysis.

Microchemical maps of vegetal tissues can also provide useful information for the analysts interested on the direct determination of macro-, micronutrients and beneficial elements when aiming at plant nutrition diagnosis. Guerra *et al.*[17] obtained P, Ca, Mg, Fe, Mn, B and Si maps in dried sugar cane leaf fragments by LIBS. The spatial distributions of the inorganic nutrients over the leaves were taken into account in the proposition of the most appropriate sampling protocol for the direct analysis of the unground leaves by both EDXRF and LIBS systems (**Figure 2**).

5 – Conclusions and perspectives

Future developments in LIBS and XRF will continue to focus on reducing the extent of matrix effects on the accuracy of the predictive calibration models. Meanwhile, alternative external calibration approaches by using matrix-matched standards previously analysed by a validated reference method are still recommended and should be extended to other crops, such as citrus, soybean and maize, since it can provide reliable results for both LIBS and XRF. Although it has been little investigated, the combination of LIBS and XRF is a promising approach aiming at the routine analysis of plant materials towards plant nutrition diagnosis. In addition, cross-validation between both techniques is feasible and a very attractive option, since similar test portions can be analyzed by them either for bulk analysis or in the microchemical mapping.

Microchemical imaging measurements have been playing a crucial role on understanding the fate of elements within plants tissues, being decisive for the establishment of representative sampling protocols aiming at direct analysis of leaves. It is evident that μ-XRF (especially μ-SRXRF) is currently much more consolidated than LIBS for this purpose. However, it is expected that the DP-LIBS approach might improve the performance of the latter one aiming at microchemical imaging, which would represent a great advance in terms of simplicity of instrumentation.

It is expected that the multielemental and simultaneous capabilities of both LIBS and XRF (*e.g.*, possibilities to handle the entire spectra) may improve the plant nutrition diagnostic, since the interactions and balances between nutrients may unveil more comprehensive concepts into plant growth and nutritional status than the mere mass fraction data of a single nutrient. Although the analysis of pellets is the most exploited and consolidated to the date, there is a growing trend in applications aiming at the direct plant analysis for nutrition diagnosis and physiology purposes, which may provide *in situ*, *in vivo* and real time analytical information. In addition, the data fusion approach *i.e.*, the combination of analytical information gathered from two or more sensors (*e.g.*, LIBS, XRF, NIR, Raman spectroscopy, Chl *a* fluorescence) to produce a more complete and specific database, is a promising strategy that should be deeply investigated in plant nutrition diagnosis.

Conflicts of interest

There are no conflicts of interest to declare.

Acknowledgements

Authors gratefully acknowledge financial support from Fundação de Amparo à Pesquisa do Estado de São Paulo (FAPESP; Grants 2015/06161-1, 2012/11998-0). Authors are also thankful to Conselho Nacional de Desenvolvimento Científico e Tecnológico (CNPq; Grants 475455/2013-4, 309679/2014-1), to Coordenação de Aperfeiçoamento de Pessoal de Nível Superior (CAPES), and to The National Science Foundation Major Research Instrumentation Program (Grant MRI-1429544).

References

1. A. V. Barker and D. J. Pilbeam, *Handbook of Plant Nutrition*, CRC Press, Boca Raton. 2015.

2. E. A. H. Pilon-Smits, C. F. Quinn, W. Tapken, M. Malagoli and M. Schiavon, *Curr. Opin. Plant Biol.*, 2009, **12**, 267-274.

3. D. Santos Jr, L. C. Nunes, G. G. Arantes de Carvalho, M. S. Gomes, F. O. Leme, P. F. Souza, L. G. C. Santos and F. J. Krug, *Spectrochim. Acta Part B*, 2012, **71-72**, 3-13.

4. R. N. Roy, A. Finck, G. J. Blair and H. L. S. Tandon, *Plant nutrition for food security - A guide for integrated nutrient management*, Food and Agriculture Organization of the United Nations, Rome. 2006.

5. S. Husted, D. P. Persson, K. H. Laursen, T. H. Hansen, P. Pedas, M. Schiller, J. N. Hegelund and J. K. Schjoerring, *J. Anal. At. Spectrom.*, 2011, **26**, 52-79.

6. P. F. Souza, D. Santos Jr, G. G. Arantes de Carvalho, L. C. Nunes, M. S. Gomes, M. B. B. Guerra and F. J. Krug, *Spectrochim. Acta Part B*, 2013, **83-84**, 61-65.

7. IPNI, *International Plant Nutrition Institute. Georgia, USA.*, Available at http://www.ipni.net.

8. M. B. B. Guerra, C. E. G. R. Schaefer, G. G. Arantes de Carvalho, P. F. de Souza, D. S. Junior, L. C. Nunes and F. J. Krug, *J. Anal. At. Spectrom.*, 2013, **28**, 1096-1101.

9. S. Reidinger, M. H. Ramsey and S. E. Hartley, *New Phytol.*, 2012, **195**, 699-706.

10. M. van Maarschalkerweerd and S. Husted, *Front. Plant Sci.*, 2015, **6**, 1-14.

11. S. A. Oliveira, in *Cerrado: correção do solo e adubação*, ed. D. M. G. Sousa and E. Lobato, Embrapa Informação Tecnológica, Brasília. 2014, pp. 245-256.

12. M. A. Belarra, M. Resano, F. Vanhaecke and L. Moens, *TrAC Trends Anal. Chem.*, 2002, **21**, 828-839.

13. J. D. Winefordner, I. B. Gornushkin, T. Correll, E. Gibb, B. W. Smith and N. Omenetto, *J. Anal. At. Spectrom.*, 2004, **19**, 1061-1083.

14. D. W. Hahn and N. Omenetto, *Appl. Spectrosc.*, 2010, **64**, 335A-366A.

15. D. W. Hahn and N. Omenetto, *Appl. Spectrosc.*, 2012, **66**, 347-419.

16. F. J. Fortes, J. Moros, P. Lucena, L. M. Cabalin and J. Javier Laserna, *Analytical Chemistry*, 2013, **85**, 640-669.

17. M. B. B. Guerra, A. Adame, E. de Almeida, G. G. Arantes de Carvalho, M. A. S. Brasil, D. Santos Jr and F. J. Krug, *J. Anal. At. Spectrom.*, 2015, **30**, 1646-1654.

18. J. Peng, F. Liu, F. Zhou, K. Song, C. Zhang, L. Ye and Y. He, *TrAC Trends Anal. Chem.*, 2016, **85**, 260-272.

19. E. Marguí, I. Queralt and M. Hidalgo, *TrAC Trends Anal. Chem.*, 2009, **28**, 362-372.

20. P. Handson and B. Shelley, *Aust. J. Exp. Agric.* , 1993, **33** 1029-1038.

21. J. Rakovský, P. Čermák, O. Musset and P. Veis, *Spectrochim. Acta Part B*, 2014, **101**, 269-287.

22. M. B. B. Guerra, E. Almeida, G. G. Arantes de Carvalho, P. F. de Souza, L. C. Nunes, D. Santos Jr and F. J. Krug, *J. Anal. At. Spectrom.*, 2014, **29**, 1667-1674.

23. G. G. Arantes de Carvalho, D. Santos Jr, L. C. Nunes, M. S. Gomes, F. O. Leme and F. J. Krug, *Spectrochim. Acta Part B*, 2012, **74–75**, 162-168.

24. M. S. Gomes, G. G. Arantes de Carvalho, D. Santos Jr and F. J. Krug, *Spectrochim. Acta Part B*, 2013, **86**, 137-141.

25. G. G. Arantes de Carvalho, J. Moros, D. Santos Jr, F. J. Krug and J. J. Laserna, *Anal. Chim. Acta*, 2015, **876**, 26-38.

26. O. Samek, J. Lambert, R. Hergenroder, M. Liska, J. Kaiser, K. Novotny and S. Kukhlevsky, *Laser Phys. Lett.*, 2006, **3**, 21-25.

27. J. A. Aguilera and C. Aragón, *Spectrochim. Acta Part B*, 2008, **63**, 793-799.

28. E. Malavolta, G. C. Vitti and S. A. Oliveira, *Avaliação do estado nutricional das plantas - princípios e aplicações*, Potafos, Piracicaba. 1997.

29. M. Pouzar, T. Cernohorsky, M. Prusova, P. Prokopcakova and A. Krejcova, *J. Anal. At. Spectrom.*, 2009, **24**, 953-957.

30. L. Krajcarová, K. Novotný, M. Kummerová, J. Dubová, V. Gloser and J. Kaiser, *Talanta*, 2017, **173**, 28-35.

31. G. Nicolodelli, G. S. Senesi, A. C. Ranulfi, B. S. Marangoni, A. Watanabe, V. de Melo Benites, P. P. A. de Oliveira, P. Villas-Boas and D. M. B. P. Milori, *Microchem. J.*, 2017, **133**, 272-278.

32. E. Tognoni and G. Cristoforetti, *J. Anal. At. Spectrom.*, 2014, **29**, 1318-1338.

33. J. Goldstein, D. E. Newbury, D. C. Joy, C. E. Lyman, P. Echlin, E. Lifshin, L. Sawyer and J. R. Michael, *Scanning Electron Microscopy and X-ray Microanalysis*, Springer, New York. 2003.

34. R. E. Van Grieken and A. A. Markowicz, *Handbook of X-Ray Spectrometry - Second Edition, Revised and Expanded*, Marcel Dekker Inc., New York. 2002.

35. M. S. Blonski, C. R. Appoloni, P. S. Parreira, P. H. A. Aragão and V. F. Nascimento Filho, *Braz. Arch. Biol. Technol.*, 2007, **50**, 851-860.

36. A. P. Marques, M. C. Freitas, H. T. Wolterbeek, T. G. Verburg and J. J. M. De Goeij, *Nucl. Instrum. Meth. Phys. Res. B*, 2007, **255**, 380-394.

37. S. Maeo, M. Krämer and K. Taniguchi, *Rev. Sci. Instrum.*, 2009, **80**, 033108.

38. W. Liu, G. E. Ice, J. Z. Tischler, A. Khounsary, C. Liu, L. Assoufid and A. T. Macrander, *Rev. Sci. Instrum.*, 2005, **76**, 113701.

39. A. Bjeoumikhov, N. Langhoff, S. Bjeoumikhova and R. Wedell, *Rev. Sci. Instrum.*, 2005, **76**, 063115.

40. S. Kazushi, M. Eisuke and H. Yasuharu, *IOP Conf. Series: Mat. Sci. Eng.*, 2011, **24**, 012018.

41. H. C. N. Tolentino, M. M. Soares, C. A. Perez, F. C. Vicentin, D. B. Abdala, D. Galante, V. C. Teixeira, D. H. C. de Araújo and H. Westfahl Jr, *J. Phys.: Conf. Series*, 2016, **849**, 012057.

42. K. Tsuji, T. Matsuno, Y. Takimoto, M. Yamanashi, N. Kometani, Y. C. Sasaki, T. Hasegawa, S. Kato, T. Yamada, T. Shoji and N. Kawahara, *Spectrochim. Acta Part B*, 2015, **113**, 43-53.

43. S. H. Nowak, A. Bjeoumikhov, J. von Borany, J. Buchriegler, F. Munnik, M. Petric, A. D. Renno, M. Radtke, U. Reinholz, O. Scharf, L. Strüder, R. Wedell and R. Ziegenrücker, *X-Ray Spectrom.*, 2015, **44**, 135-140.

44. E. P. Bertin, *Principles and practice of X-ray spectrometric analysis*, Plenum Press, New York, USA, 1971.

45. G. G. Arantes de Carvalho, D. Santos Jr, M. S. Gomes, L. C. Nunes, M. B. B. Guerra and F. J. Krug, *Spectrochim. Acta Part B*, 2015, **105**, 130–135.

46. R. Sitko and B. Zawisza, in *X-Ray Spectroscopy*, ed. S. K. Sharma, InTech, Rijeka. 2012, pp. 137-162.

47. L. C. Nunes, J. W. B. Braga, L. C. Trevizan, P. F. Souza, G. G. Arantes de Carvalho, D. Santos Jr, R. J. Poppi and F. J. Krug, *J. Anal. At. Spectrom.*, 2010, **25**, 1453-1460.

48. J. Benton Jones Jr, in *Handbook of reference methods for plant analysis*, ed. Y. P. Kalra, CRC Press, Boca Raton. 1998, pp. 25-35.

49. M. S. Gomes, D. Santos Jr, L. C. Nunes, G. G. Arantes de Carvalho, F. O. Leme and F. J. Krug, *Talanta*, 2011, **85**, 1744-1750.

50. R. Zeisler, *Fres. J. Anal. Chem.*, 1998, **360**, 376-379.

51. B. Tischer, R. G. Vendruscolo, R. Wagner, C. R. Menezes, C. S. Barin, S. R. Giacomelli, J. M. Budel and J. S. Barin, *Chem. Pap.*, 2017, **71**, 753-761.

52. B. Markert, *Sci. Total Environ.*, 1995, **176**, 45-61.

53. A. Chamayou and J. A. Dodds, in *Handbook of Powder Technology*, ed. A. D. Salman, M. Ghadiri and M. J. Hounslow, Elsevier, Amsterdam. 2007, pp. 421-435.

54. J. Peng, Y. He, L. Ye, T. Shen, F. Liu, W. Kong, X. Liu and Y. Zhao, *Analytical Chemistry*, 2017, **89**, 7593-7600.

55. Q. Sun, M. Tran, B. W. Smith and J. D. Winefordner, *Can. J. Anal. Sci. Spectrosc.*, 1999, **44**, 164-170.

56. L. Arroyo, T. Trejos, P. R. Gardinali and J. R. Almirall, *Spectrochim. Acta Part B*, 2009, **64**, 16-25.

57. J. W. B. Braga, L. C. Trevizan, L. C. Nunes, I. A. Rufini, D. Santos Jr and F. J. Krug, *Spectrochim. Acta Part B*, 2010, **65**, 66-74.

58. M. A. Gondal, T. Hussain, Z. H. Yamani and M. A. Baig, *Talanta*, 2007, **72**, 642-649.

59. S. C. Jantzi, V. Motto-Ros, F. Trichard, Y. Markushin, N. Melikechi and A. De Giacomo, *Spectrochim. Acta Part B*, 2016, **115**, 52-63.

60. J. Omote, H. Kohno and K. Toda, *Anal. Chim. Acta*, 1995, **307**, 117-126.

61. G. Takahashi, *Rigaku J.*, 2015, **31**, 26-30.

62. Z. Üstündağ, *Spectrosc. Lett.*, 2009, **42**, 7-11.

63. I. Queralt, M. Ovejero, M. L. Carvalho, A. F. Marques and J. M. Llabrés, *X-Ray Spectrom.*, 2005, **34**, 213-217.

64. L. C. Peruchi, L. C. Nunes, G. G. Arantes de Carvalho, M. B. B. Guerra, E. de Almeida, I. A. Rufini, D. Santos and F. J. Krug, *Spectrochim. Acta Part B*, 2014, **100**, 129-136.

65. D. Knudsen, R. B. Clark, J. L. Denning and P. A. Pier, *J. Plant Nutrit.*, 1981, **3**, 61-75.

66. M. Fiori, *J. Radioanal. Nucl. Chem.*, 2001, **249**, 509-512.

67. N. G. Paltridge, L. J. Palmer, P. J. Milham, G. E. Guild and J. C. R. Stangoulis, *Plant Soil*, 2012, **361**, 251-260.

68. C. S. Nomura, D. Santos Jr, L. C. Nunes, M. B. B. Guerra, G. G. Arantes de Carvalho, P. V. Oliveira and F. J. Krug, in *Métodos de Preparo de Amostras para Análise Elementar*, ed. F. J. Krug and F. R. P. Rocha, EditSBQ, São Paulo. 2016, pp. 139-196.

69. N. Miliszkiewicz, S. Walas and A. Tobiasz, *J. Anal. At. Spectrom.*, 2015, **30**, 327-338.

70. E. Marguí, M. Hidalgo and I. Queralt, *Spectrochim. Acta Part B*, 2005, **60**, 1363-1372.

71. E. V. Chuparina and M. G. Azovsky, *Anal. Lett.*, 2016, **49**, 1963-1973.

72. L. C. Trevizan, D. Santos Jr, R. E. Samad, N. D. Vieira Jr, C. S. Nomura, L. C. Nunes, I. A. Rufini and F. J. Krug, *Spectrochim. Acta Part B*, 2008, **63**, 1151-1158.

73. L. C. Trevizan, D. Santos Jr, R. E. Samad, N. D. Vieira Jr, L. C. Nunes, I. A. Rufini and F. J. Krug, *Spectrochim. Acta Part B*, 2009, **64**, 369-377.

74. N. G. Paltridge, P. J. Milham, J. I. Ortiz-Monasterio, G. Velu, Z. Yasmin, L. J. Palmer, G. E. Guild and J. C. R. Stangoulis, *Plant Soil*, 2012, **361**, 261-269.

75. G. S. Senesi, M. Dell'Aglio, A. De Giacomo, O. De Pascale, Z. A. Chami, T. M. Miano and C. Zaccone, *CLEAN – Soil, Air, Water*, 2014, **42**, 791-798.

76. E. Marguí, I. Queralt, M. L. Carvalho and M. Hidalgo, *Anal. Chim. Acta*, 2005, **549**, 197-204.

77. L. A. Kalcsits, *Front. Plant Sci.*, 2016, **7**, 1-8.

78. T. Tezotto, J. L. Favarin, A. P. Neto, P. L. Gratão, R. A. Azevedo and P. Mazzafera, *Scientia Agricola*, 2013, **70**, 263-267.

79. N. V. Campos, M. B. B. Guerra, J. W. V. Mello, C. E. G. R. Schaefer, F. J. Krug, E. E. N. Alves and A. A. Azevedo, *J. Anal. At. Spectrom.*, 2015, **30**, 2375-2383.

80. H. Mark, *Principles and Practice of Spectroscopic Calibration*, John Wiley & Sons, Inc., New York. 1991.

81. P. J. Jenks, *Spectrosc. Europe*, 2014, **26**, 22-23.

82. H. W. Vesper, W. G. Miller and G. L. Myers, *The Clinical Biochemistry Reviews*, 2007, **28**, 139-147.

83. J. M. Robinson, S. R. Barrett, K. Nhoy, R. K. Pandey, J. Phillips, O. M. Ramirez and R. I. Rodriguez, *Energy Fuels*, 2009, **23**, 2235-2241.

84. R. N. Feudale, N. A. Woody, H. Tan, A. J. Myles, S. D. Brown and J. Ferré, *Chemometr. Intell. Lab. Syst.*, 2002, **64**, 181-192.

85. P. Porizka, J. Klus, A. Hrdlicka, J. Vrabel, P. Skarkova, D. Prochazka, J. Novotny, K. Novotny and J. Kaiser, *J. Anal. At. Spectrom.*, 2017, **32**, 277-288.

86. P. Geladi and B. R. Kowalski, *Anal. Chim. Acta*, 1986, **185**, 1-17.

87. P. Valderrama, J. W. B. Braga and R. J. Poppi, *J. Agric. Food Chem.*, 2007, **55**, 8331-8338.

88. B. Walczak and D. L. Massart, *Chemometr. Intelligent Lab. Syst.*, 1998, **41**, 1-15.

89. K. Devey, M. Mucalo, G. Rajendram and J. Lane, *Commun. Soil Sci. Plant Anal.*, 2015, **46**, 72-80.

90. S. Awasthi, R. Kumar, A. Devanathan, R. Acharya and A. K. Rai, *Anal. Chem. Res.*, 2017, **12**, 10-16.

91. M. Markiewicz-Keszycka, X. Cama-Moncunill, M. P. Casado-Gavalda, Y. Dixit, R. Cama-Moncunill, P. J. Cullen and C. Sullivan, *Trends Food Sci. Technol.*, 2017, **65**, 80-93.

92. G. Kim, J. Kwak, J. Choi and K. Park, *J. Agric. Food Chem.*, 2012, **60**, 718-724.

93. D. M. Silvestre, F. M. Barbosa, B. T. Aguiar, F. O. Leme and C. S. Nomura, *Anal. Chem. Res.*, 2015, **5**, 28-33.

94. J. Sherman, *Spectrochim. Acta*, 1955, **7**, 283-306.

95. V. Thomsen, *Spectroscopy*, 2007, **22**, 46-50.

96. A. A. Shaltout, M. A. Moharram and N. Y. Mostafa, *Spectrochim. Acta Part B*, 2012, **67**, 74-78.

97. L. K. Andersen, T. J. Morgan, A. K. Boulamanti, P. Álvarez, S. V. Vassilev and D. Baxter, *Energy Fuels*, 2013, **27**, 7439-7454.

98. J. Leroux and M. Mahmud, *Analytical Chemistry*, 1966, **38**, 76-82.

99. S. M. Simabuco and V. F. Nascimento Filho, *Scientia Agricola*, 1994, **51**, 197-206.

100. A. Lubecki, *J. Radioanal. Chem.*, 1969, **3**, 317-328.

101. E. Tognoni, G. Cristoforetti, S. Legnaioli and V. Palleschi, *Spectrochim. Acta Part B*, 2010, **65**, 1-14.

102. S. Ma, X. Gao, K. Guo, M. Kahsay and J. Lin, *Sci. China - Phys., Mechan. Astron.*, 2011, **54**, 1953–1957.

103. J. Kaiser, K. Novotny, M. Z. Martin, A. Hrdlicka, R. Malina, M. Hartl, V. Adam and R. Kizek, *Surf. Sci. Rep.*, 2012, **67**, 233-243.

104. R. S. Harmon, R. E. Russo and R. R. Hark, *Spectrochim. Acta Part B*, 2013, **87**, 11-26.

105. D. W. Hahn, *Spectrosc.*, 2009, **24**, 26-33.

106. H. Jull, R. Künnemeyer and P. Schaare, Precision Agric., 2018, https://doi.org/10.1007/s11119-018-9559-4.

107. M. Barbafieri, R. Pini, A. Ciucci and E. Tassi, *Chem. Ecol.*, 2011, **27**, 161-169.

108. M. M. El-Deftar, J. Robertson, S. Foster and C. Lennard, *Forensic Sci. Int.*, 2015, **251**, 95-106.

109. M. A. Gondal, Y. B. Habibullah, U. Baig and L. E. Oloore, *Talanta*, 2016, **152**, 341-352.

110. E. K. Towett, K. D. Shepherd and B. Lee Drake, *X-Ray Spectrom.*, 2016, **45**, 117-124.

111. T. I. McLaren, C. N. Guppy and M. K. Tighe, *Soil Sci. Soc. Am. J.*, 2012, **76**, 1446-1453.

112. E. Marguí, M. Hidalgo and I. Queralt, *Spectroscopy Europe*, 2007, **19**, 12-17.

113. A. Aberoumand, *Food Anal. Meth.*, 2009, **2**, 204-207.

114. A. Khuder, M. K. Sawan, J. Karjou and A. K. Razouk, *Spectrochim. Acta Part B*, 2009, **64**, 721-725.

115. S. Al-Omari, *X-Ray Spectrom.*, 2011, **40**, 31-36.

116. K. Demir, O. Sahin, Y. K. Kadioglu, D. J. Pilbeam and A. Gunes, *Scientia Horticulturae*, 2010, **127**, 16-22.

117. E. V. Chuparina and T. S. Aisueva, *Environ. Chem. Lett.*, 2011, **9**, 19-23.

118. P. Nayak, P. R. Behera, M. Thirunavoukkarasu and P. K. Chand, *Appl. Rad. Isotop.*, 2011, **69**, 567-573.

119. E. P. Khramova, I. G. Boyarskikh, O. V. Chankina and K. P. Kutsenogii, *J. Surf. Investig. X-ray, Synchrotron Neutr. Tech.*, 2012, **6**, 454-457.

120. O. Sahin, M. B. Taskin, Y. K. Kadioglu, A. Inal, D. J. Pilbeam and A. Gunes, *J. Plant Nutrit.*, 2014, **37**, 458-468.

121. T. H. Dao, *Comput. Electron. Agric*., 2016, **129**, 84-90.

122. T. H. Dao, *Precision Agric*., 2017, **18**, 685-700.

123. M. B. B. Guerra, A. Adame, E. Almeida, M. A. S. Brasil, C. E. G. R. Schaefer and F. J. Krug, *J. Braz. Chem. Soc*., 2018, **29**, 1086-1093.

124. B. Wu and J. S. Becker, *Metallomics*, 2012, **4**, 403-416.

125. J. S. Becker, in *Meth. Mol. Biol.* 2010, vol. 656, pp. 51-82.

126. A. Sussulini and J. S. Becker, *Mass Spectrom. Rev.*, 2017, **36**, 47-57.

127. B. Q. Huang and E. C. Yeung, in *Plant Microtechniques and Protocols*, ed. E. C. T. Yeung, C. Stasolla, M. J. Sumner and B. Q. Huang, Springer International Publishing, Cham. 2015, pp. 23-43.

128. H. A. Castillo-Michel, C. Larue, A. E. Pradas del Real, M. Cotte and G. Sarret, *Plant Physiol. Biochem.*, 2017, **110**, 13-32.

129. N. Fukuda, A. Hokura, N. Kitajima, Y. Terada, H. Saito, T. Abe and I. Nakai, *J. Anal. At. Spectrom.*, 2008, **23**, 1068-1075.

130. S. Jiménez, F. Morales, A. Abadía, J. Abadía, M. A. Moreno and Y. Gogorcena, *Plant Soil*, 2008, **315**, 93-106.

131. E. Marguí, A. Jurado, M. Hidalgo, G. Pardini, M. Gispert and I. Queralt, *Appl. Spectrosc.*, 2009, **63**, 1396-1402.

132. N. Tomasi, C. Rizzardo, R. Monte, S. Gottardi, N. Jelali, R. Terzano, B. Vekemans, M. De Nobili, Z. Varanini, R. Pinton and S. Cesco, *Plant Soil*, 2009, **325**, 25-38.

133. S. Tian, L. Lu, X. Yang, S. M. Webb, Y. Du and P. H. Brown, *Environ. Sci. Technol.*, 2010, **44**, 5920-5926.

134. P. M. Kopittke, N. W. Menzies, M. D. de Jonge, B. A. McKenna, E. Donner, R. I. Webb, D. J. Paterson, D. L. Howard, C. G. Ryan, C. J. Glover, K. G. Scheckel and E. Lombi, *Plant Physiol.*, 2011, **156**, 663-673.

135. A. L. Seyfferth, S. M. Webb, J. C. Andrews and S. Fendorf, *Geochim. Cosmochim. Acta*, 2011, **75**, 6655-6671.

136. A. D. Servin, H. Castillo-Michel, J. A. Hernandez-Viezcas, B. C. Diaz, J. R. Peralta-Videa and J. L. Gardea-Torresdey, *Environ. Sci. Technol.*, 2012, **46**, 7637-7643.

137. J. A. Hernandez-Viezcas, H. Castillo-Michel, J. C. Andrews, M. Cotte, C. Rico, J. R. Peralta-Videa, Y. Ge, J. H. Priester, P. A. Holden and J. L. Gardea-Torresdey, *ACS Nano*, 2013, **7**, 1415-1423.

138. J. Song, Y. Q. Yang, S. H. Zhu, G. C. Chen, X. F. Yuan, T. T. Liu, X. H. Yu and J. Y. Shi, *Biologia Plantarum*, 2013, **57**, 581-586.

139. P. M. Kopittke, M. D. de Jonge, P. Wang, B. A. McKenna, E. Lombi, D. J. Paterson, D. L. Howard, S. A. James, K. M. Spiers, C. G. Ryan, A. A. T. Johnson and N. W. Menzies, *New Phytol.*, 2014, **201**, 1251-1262.

140. Y. Ma, P. Zhang, Z. Zhang, X. He, Y. Li, J. Zhang, L. Zheng, S. Chu, K. Yang, Y. Zhao and Z. Chai, *Nanotoxicol.*, 2015, **9**, 262-270.

141. B. Meng, X. Feng, G. Qiu, C. W. N. Anderson, J. Wang and L. Zhao, *Environ. Sci. Technol.*, 2014, **48**, 7974-7981.

142. Y. Chen, K. L. Moore, A. J. Miller, S. P. McGrath, J. F. Ma and F.-J. Zhao, *J. Experim. Bot.*, 2015, **66**, 3717-3724.

143. H. Neidhardt, U. Kramar, X. Tang, H. Guo and S. Norra, *Chemie der Erde - Geochem.*, 2015, **75**, 261-270.

144. S. Tian, L. Lu, R. Xie, M. Zhang, J. Jernstedt, D. Hou, C. Ramsier and P. Brown, *Front. Plant Sci.*, 2015, **5**, 1-9.

145. L. Zanin, N. Tomasi, C. Rizzardo, S. Gottardi, R. Terzano, M. Alfeld, K. Janssens, M. De Nobili, T. Mimmo and S. Cesco, *Physiologia Plantarum*, 2015, **154**, 82-94.

146. L. Zhao, Y. Sun, J. A. Hernandez-Viezcas, J. Hong, S. Majumdar, G. Niu, M. Duarte-Gardea, J. R. Peralta-Videa and J. L. Gardea-Torresdey, *Environ. Sci. Technol.*, 2015, **49**, 2921-2928.

147. H. Gallardo, I. Queralt, J. Tapias, M. Guerra, M. L. Carvalho and E. Marguí, *J. Food Comp. Anal.*, 2016, **50**, 1-9.

148. I. Ramos, I. M. Pataco, M. P. Mourinho, F. Lidon, F. Reboredo, M. F. Pessoa, M. L. Carvalho, J. P. Santos and M. Guerra, *Spectrochim. Acta Part B*, 2016, **120**, 30-36.

149. L. Lu, R. Xie, T. Liu, H. Wang, D. Hou, Y. Du, Z. He, X. Yang, H. Sun and S. Tian, *Chemosphere*, 2017, **175**, 356-364.

150. J. Trebolazabala, M. Maguregui, H. Morillas, A. de Diego and J. M. Madariaga, *Microchem. J.*, 2017, **131**, 137-144.

151. M. J. Talbot and R. G. White, *Plant Methods*, 2013, **9**, 36-42.

152. R. Thavarajah, V. Mudimbaimannar, J. Elizabeth, U. Rao and K. Ranganathan, *J. Oral Maxillofac. Pathol.*, 2012, **16**, 400-405.

153. H. Roschzttardtz, L. Grillet, M. P. Isaure, G. Conéjéro, R. Ortega, C. Curie and S. Mari, *J. Biol. chem.*, 2011, **286**, 27863-27866.

154. D. Studer, W. Graber, A. Al-Amoudi and P. Eggli, *J. Microsc.*, 2001, **203**, 285-294.

155. K. E. Smart, J. A. C. Smith, M. R. Kilburn, B. G. H. Martin, C. Hawes and C. R. M. Grovenor, *Plant J.*, 2010, **63**, 870-879.

156. S. Mishra, G. Wellenreuther, J. Mattusch, H.-J. Stärk and H. Küpper, *Plant Physiol.*, 2013, **163**, 1396-1408.

157. G. Sarret, E. Harada, Y. E. Choi, M. P. Isaure, N. Geoffroy, S. Fakra, M. A. Marcus, M. Birschwilks, S. Clemens and A. Manceau, *Plant Physiol.*, 2006, **141**, 1021-1034.

158. R. R. Brooks, J. Lee, R. D. Reeves and T. Jaffre, *J. Geochem. Explor.*, 1977, **7**, 49-57.

159. T. Jaffré, R. R. Brooks, J. Lee and R. D. Reeves, *Science*, 1976, **193**, 579-580.

160. A. van der Ent, A. J. M. Baker, R. D. Reeves, A. J. Pollard and H. Schat, *Plant Soil*, 2013, **362**, 319-334.

161. N. Rascio and F. Navari-Izzo, *Plant Sci.*, 2011, **180**, 169-181.

162. H. Ali, E. Khan and M. A. Sajad, *Chemosphere*, 2013, **91**, 869-881.

163. D. E. Salt, R. D. Smith and I. Raskin, *Annu. Rev. Plant Physiol. Plant Mol. Biol.*, 1998, **49**, 643-668.

164. R. R. Brooks, M. F. Chambers, L. J. Nicks and B. H. Robinson, *Trends Plant Sci.*, 1998, **3**, 359-362.

165. V. Sheoran, A. S. Sheoran and P. Poonia, *Miner. Eng.*, 2009, **22**, 1007-1019.

166. V. Sheoran, A. S.Sheoran and P. Poonia, *J. Geochem. Explor.*, 2013, **128**, 42-50.

167. R. G. Haverkamp and A. T. Marshall, *J. Nanopart. Res.*, 2009, **11**, 1453-1463.

168. J. L. Gardea-Torresdey, E. Rodriguez, J. G. Parsons, J. R. Peralta-Videa, G. Meitzner and G. Cruz-Jimenez, *Anal. Bioanal. Chem.*, 2005, **382**, 347-352.

169. J. A. Howe, R. H. Loeppert, V. J. DeRose, D. B. Hunter and P. M. Bertsch, *Environ. Sci. Technol.*, 2003, **37**, 4091-4097.

170. A. van der Ent, W. J. Przybyłowicz, M. D. de Jonge, H. H. Harris, C. G. Ryan, G. Tylko, D. J. Paterson, A. D. Barnabas, P. M. Kopittke and J. Mesjasz-Przybyłowicz, *New Phytol*., 2018, **218**, 432-452.

171. A. D. Surowka, P. Wrobel, M. M. Marzec, D. Adamek and M. Szczerbowska-Boruchowska, *Spectrochim. Acta Part B*, 2016, **123**, 47-58.

172. T. Punshon, M. L. Guerinot and A. Lanzirotti, *Ann. Bot.*, 2009, **103**, 665-672.

173. P. Vijayan, I. R. Willick, R. Lahlali, C. Karunakaran and K. K. Tanino, *Plant Cell Physiol.*, 2015, **56**, 1252-1263.

174. F.-J. Zhao, K. L. Moore, E. Lombi and Y.-G. Zhu, *Trends Plant Sci.*, 2014, **19**, 183-192.

175. Z. Abdullaeva, in *Nanomaterials in Daily Life: Compounds, Synthesis, Processing and Commercialization*, Springer International Publishing, Cham. 2017, pp. 47-65.

176. A. Vedda and I. Villa, in *Nano-Optics: Principles Enabling Basic Research and Applications*, ed. B. Di Bartolo, J. Collins and L. Silvestri, Springer Netherlands, Dordrecht. 2017, pp. 369-386.

177. S. A. Ntim and G. O. Noonan, in *Nanotechnologies in Food*, The Royal Society of Chemistry, 2 edn. 2017, pp. 118-142.

178. I. Iavicoli, V. Leso, D. H. Beezhold and A. A. Shvedova, *Toxicol. Appl. Pharmacol.*, 2017, **329**, 96-111.

179. F. M. Verbi Pereira and D. M. B. P. Milori, *J. Anal. At. Spectrom.*, 2010, **25**, 351-355.

180. D. Romero and J. J. Laserna, *Analytical Chemistry*, 1997, **69**, 2871-2876.

181. V. Piñon, M. P. Mateo and G. Nicolas, *Appl. Spectrosc. Rev.*, 2013, **48**, 357-383.

182. J. M. Vadillo and J. J. Laserna, in *Laser-induced breakdown spectroscopy (LIBS) - Fundamentals and applications*, ed. A. W. Miziolek, V. Palleschi and I. Schechter, Cambridge University Press, New York. 2006, pp. 254-281.

183. R. E. Russo, X. Mao, J. L. Gonzalez and J. Yoo, *Spectroscopy*, 2013, **28**, 24-39.

184. E. L. Gurevich and R. Hergenroeder, *Appl. Spectrosc.*, 2007, **61**, 233A-242A.

185. H. Hou, L. Cheng, T. Richardson, G. Chen, M. Doeff, R. Zheng, R. Russo and V. Zorba, *J. Anal. At. Spectrom.*, 2015, **30**, 2295-2302.

186. J. Koch and D. Güenther, *Appl. Spectrosc.*, 2011, **65**, 155A-162A.

187. O. Samek, V. Margetic and R. Hergenröder, *Anal. Bioanal. Chem.*, 2005, **381**, 54-56.

188. T. A. Labutin, V. N. Lednev, A. A. Ilyin and A. M. Popov, *J. Anal. At. Spectrom.*, 2016, **31**, 90-118.

189. O. Samek, V. Margetic, N. von Wirén, A. Michels, K. Niemax and R. Hergenröder, *Appl. Phys. A*, 2004, **79**, 957-960.

190. J. Kaiser, O. Samek, L. Reale, M. Liska, R. Malina, A. Ritucci, A. Poma, A. Tucci, F. Flora, A. Lai, L. Mancini, G. Tromba, F. Zanini, A. Faenov, T. Pikuz and G. Cinque, *Microsc. Res. Techniq.*, 2007, **70**, 147-153.

191. A. Assion, M. Wollenhaupt, L. Haag, F. Mayorov, C. Sarpe-Tudoran, M. Winter, U. Kutschera and T. Baumert, *Appl. Phys. B*, 2003, **77**, 391-397.

192. M. Galiová, J. Kaiser, K. Novotný, M. Hartl, R. Kizek and P. Babula, *Microsc. Res. Tech.*, 2011, **74**, 845-852.

193. M. Galiová, J. Kaiser, K. Novotný, J. Novotný, T. Vaculovič, M. Liška, R. Malina, K. Stejskal, V. Adam and R. Kizek, *Appl. Phys. A*, 2008, **93**, 917-922.

194. M. Galiová, J. Kaiser, K. Novotný, O. Samek, L. Reale, R. Malina, K. Páleníková, M. Liska, V. Cudek, V. Kanický, V. Otruba, A. Poma and A. Tucci, *Spectrochim. Acta Part B*, 2007, **62**, 1597-1605.

195. J. Kaiser, M. Galiová, K. Novotný, R. Cervenka, L. Reale, J. Novotný, M. Liska, O. Samek, V. Kanický, A. Hrdlicka, K. Stejskal, V. Adam and R. Kizek, *Spectrochim. Acta Part B*, 2009, **64**, 67-73.

196. S. Krizkova, P. Ryant, O. Krystofova, V. Adam, M. Galiova, M. Beklova, P. Babula, J. Kaiser, K. Novotny, J. Novotny, M. Liska, R. Malina, J. Zehnalek, J. Hubalek, L. Havel and R. Kizek, *Sensors*, 2008, **8**, 445-463.

197. O. Krystofova, V. Shestivska, M. Galiova, K. Novotny, J. Kaiser, J. Zehnalek, P. Babula, R. Opatrilova, V. Adam and R. Kizek, *Sensors*, 2009, **9**, 5040-5058.

198. Y. Gimenez, B. Busser, F. Trichard, A. Kulesza, J. M. Laurent, V. Zaun, F. Lux, J. M. Benoit, G. Panczer, P. Dugourd, O. Tillement, F. Pelascini, L. Sancey and V. Motto-Ros, *Sci. Rep.*, 2016, **6**, 29936.

199. C. Zhao, D. Dong, X. Du and W. Zheng, *Sensors*, 2016, **16**, 1764.

LIST OF ACRONYMS AND ABBREVIATIONS

CCD - charge-coupled device

CF-LIBS – calibration free laser-induced breakdown spectroscopy

Chl - chlorophyll

CRM – certified reference material

DAP - days after planting

ENMs - engineered nanomaterials

EDPXRF – energy-dispersive polarized X-ray fluorescence spectrometry

FP - fundamental parameters

fs-LIBS – femtosecond laser-induced breakdown spectroscopy

HCA - hierarchical cluster analysis

KNN – K-nearest neighbour

ICCD - intensified charge-coupled device

ICP OES – inductively coupled plasma optical emission spectrometry

IR – infrared

LA-ICP-MS – laser ablation inductively coupled plasma mass spectrometry

LIBS – laser-induced breakdown spectroscopy

LIP - laser-induced plasmas

LOD – limit of detection

NPs – nanoparticles

ns - nanosecond

ns-LIBS - nanosecond laser-induced breakdown spectroscopy

OES - optical emission spectrometry

PCA - principal component analysis

PLS - partial least squares

PLS-DA - partial least squares discriminant analysis

P-XRF - portable X-ray fluorescence spectrometry

SDD - silicon drift detector

SIMCA - soft independent modelling of class analogies

SIMS - secondary ion mass spectrometry

SR - sufficiency ranges

td – delay time

TVD - top visible dewlap

ti – integration time gate

UV - ultraviolet

XAS - X-ray absorption spectroscopy

XRF - X-ray fluorescence spectrometry

WDXRF – wavelength-dispersive X-ray fluorescence spectrometry

Z - atomic number

μ-EDXRF - micro energy-dispersive X-ray fluorescence spectrometry

μ-SRXRF – micro Synchrotron Radiation X-ray fluorescence spectrometry

μ-XANES – micro X-ray absorption near-edge spectroscopy

μ-XRF – micro X-ray fluorescence spectrometry

LIST OF TABLES

Table 1 - Sufficiency ranges of macro- and micronutrients in selected crops under adequate nutritional status. Data compiled from ref.[11,28]

Nutrient	*Sugar cane*	*Rice*	*Citrus*	*Maize*	*Soybean*	*Wheat*
Macronutrients (g kg^{-1})						
N	19 - 21	27 - 35	25 - 27	28 - 35	45 - 55	20 - 34
P	2.0 – 2.4	1.8 – 3.0	1.2 – 1.6	1.8 – 3.0	2.5 – 5.0	2.1 – 3.3
K	11 - 13	13 - 30	10 - 15	13 - 30	17 - 25	15 - 30
Ca	8 - 10	2.5 - 10	35 - 45	2.5 - 10	4.0 - 20	2.5 - 10
Mg	2.0 – 3.0	1.5 – 5.0	2.3 – 4.0	1.5 – 5.0	3.0 - 10	1.5 – 4.0
S	2.5 – 3.0	1.5 – 3.0	2.0 – 3.0	1.4 – 3.0	2.1 – 4.0	1.5 – 3.0
Micronutrients (mg kg^{-1})						
B	15 - 50	4 - 25	36 - 100	10 - 25	21 - 55	5 - 20
Cu	8 - 10	3 - 25	5 - 16	6 - 20	10 - 30	5 - 25
Fe	200 - 500	70 - 200	60 - 120	30 - 250	51 - 350	100 - 300
Mn	100 - 250	70 - 400	25 - 50	20 - 200	21 - 100	25 - 150
Mo	0.15 – 0.30	0.1 – 0.3	0.1 – 1.0	0.1 – 0.2	1.0 – 5.0	0.3 – 0.5
Zn	25 - 50	10 - 50	25 - 100	15 - 100	20 - 50	20 - 70

Table 2 – Limits of detection of LIBS and EDXRF systems obtained from the same set of ground sugar cane leaves analysed as pressed pellets. Data based on 3.3 σ

Nutrient	*LODs*				
	ns-LIBS[23]	*fs-LIBS*[25 a]	*Benchtop EDXRF*[22]	*Portable EDXRF*[22]	*Benchtop μ-EDXRF*[8]
			Macronutrients (g kg^{-1})		
N	-	-	-	-	-
P	0.01	0.4	0.10	0.25	0.50
K	2	-	0.14	0.09	0.31
Ca	0.01	0.007	0.06	0.06	0.45
Mg	0.02	0.02	-	-	-
S	-	-	0.09	0.13	0.19
			Micronutrients (mg kg^{-1})		
B	0.5	-	-	-	-
Cu	0.4	7[a]	-	-	-
Fe	0.4	12	20	20	60
Mn	0.3	2	20	20	30
Mo	-	-	-	-	-
Zn	0.2	80[a]	-	-	-

[a] Estimated from calibration model built with bean, citrus, coffee, eucalyptus, grape, lettuce, mango, pearl millet, pine needles, rubber tree, soy, spinach, sugarcane, and tomato leaves.

Table 3 - Field sampling protocols of selected crops aiming at plant nutrition diagnosis. Data compiled from ref.[11]

Crop	*Sampling period*	*Plant tissue*	*Number of samples*
Rice	Tillering season	Flag leaf	50 leaves from 50 plants
Sugar cane	Grand growth period	Third leaf or TVD[a] without a sheath	40 leaves from 40 plants
Citrus	Fruiting stages	Fully mature leaves adjacent to fruit	100 leaves from 25 plants
Maize	Tasseling to silking	Leaf opposite and below ear	30 leaves from 30 plants
Soybean	Prior to or at bloom (phenological stage R1)	Upper fully developed trifoliate leaf	30 leaves from 30 plants
Wheat	Flowering	Flag leaf	30 leaves from 30 plants

[a] TVD = Top Visible Dewlap (uppermost fully expanded leaf that has a visible dewlap or distinct collar).

Table 4 – Selected applications dealing with quantitative analysis of plant leaves by LIBS

Matrix	Analytes	Instrumentation	Calibration strategy	Sample preparation	LOD mg kg^{-1}	Ref
CRMs and leaves of Brachiaria, soya, banana, coffee, jack, maize, pepper, guayava	Ca, K, Mg, P	Nd:YAG@1064 nm, 10 Hz, 200 mJ/pulse, 23 Jcm^{-2}, 4.6 W cm^{-2}, 8 pulses, 2 µs t_d, 5 µs t_i	External calibration with CRMs	Drying, cryogenic grinding and pelletizing	10 (Ca), 2500 (K), 20 (Mg), 80 (P)	72
CRMs and leaves of soya, lettuce, endive, boldo, grass, jack, Brachiaria, coffee, mango, maize and pepper	B, Cu, Fe, Mn, Zn	Nd:YAG@1064 nm, 10 Hz, 200 mJ/pulse, 23 Jcm^{-2}, 4.6 Wcm^{-2}, 8 and 30 pulses, 2 µs t_d, 5 µs t_i	External calibration with CRMs	Drying, cryogenic grinding and pelletizing	1.4 (B), 2.5 (Cu), 2.8 (Fe), 1.1 (Mn), 1.0 (Zn)	73
CRMs and leaves of barley, poppy, wheat and rape	Ca, K, Mg, P	Nd:YAG@1064 nm, 20 Hz, double pulse, 65, 68 and 78 mJ/pulse, 30 pulses, 7 µs t_d, 1 µs t_i, atmospheric pressure	External calibration with samples analyzed by a validated reference method	Drying, cryogenic grinding and pelletizing	*n.r.*	29
Sugar cane leaves	B, Ca, Fe, K, Mg, Mn, P, Zn	Nd:YAG@1064 nm, 10 Hz, 110 mJ/pulse, 25 Jcm^{-2}, 25 pulses, 2 µs t_d, 4.5 µs t_i	External univariate and multivariate (PLS) calibrations with samples analyzed by a validated reference method	Drying, cryogenic grinding and pelletizing	30 (P), 210 (K), 80 (Ca), 120 (Mg), 6.6 (Mn), 9.5 (Fe), 1.2 (Zn), 0.8 (B)	47
CRMs and leaves of Brachiaria, soya, banana, coffee, maize, mango, pepper	B, Cu, Fe, Mn, Zn	Nd:YAG@532 nm, 10 Hz, 70 mJ/pulse, 25 Jcm^{-2}, 2.0 $GWcm^{-2}$, 30 pulses, 1.1 µs t_d, 10 µs t_i	External univariate and multivariate (PLS) calibrations with samples analyzed by a validated reference method	Drying, cryogenic grinding, mixing with cellulose binder and pelletizing	3 (B), 5 (Cu), 7 (Fe), 4 (Mn), 4 (Zn)	57
Poplar tree leaves	Ca, Fe, N, P	Ti:Sapphire@800 nm, 10 Hz, 100 fs, 25 mJ/pulse	Calibration free method	Direct analysis of dried and flattened leaves	*n.r.*	102
Mustard leaves	Pb	Nd:YAG@1064 nm, 10 Hz,	External calibration with	Drying, grinding and	*n.r.*	107

		300 mJ	samples analyzed by a validated reference method	pelletizing		
CRMs and sugar cane leaves	Al, B, Ca, Cu, Fe, K, Mg, Mn, P, Zn	Nd:YAG@1064 nm, 10 Hz, 50 Jcm^{-2}, 2.0 $GWcm^{-2}$, 20 pulses, 2 µs t_d, 5 µs t_i	External calibration with CRMs	Drying, cryogenic grinding (95% of particles < 75µm) and pelletizing	0.1 (Ca), 0.01 (Mg), 1.0 (P), 0.5 (B), 0.4 (Cu, Fe), 0.3 (Mn), 0.2 (Zn), 3.9 (Al), 2000 (K)	23
Spinach leaves	Mg, Ca, Na, K	Nd:YAG@1064 nm, 10 Hz, 80 and 140 mJ/pulse, 50 laser pulses	External calibration with NIST SRM 1570a (spinach leaves) mixed with lactose anhydrous at different ratios	Drying, grinding, sieving (50 and 200 mesh) and pelletizing	30 (Mg), 103 (Ca), 36 (Na), 44 (K)	92
Sugar cane leaves	P, K, Ca, Mg, Cu, Mn, Zn	Nd:YAG @1064 nm, 10 Hz, 110 mJ/pulse, 25 Jcm^{-2}, 25 pulses, 2 µs t_d, 5 µs t_i	External calibration with matrix-matched standards	Drying, cryogenic grinding (95% of particles < 75µm) and pelletizing	10 (Ca, Mg), 1400 (K), 30 (P), 0.8 (Mn), 1.0 (Zn), 0.6 (Cu)	24
Sugar cane leaves	Si	Nd:YAG @1064 nm, 10 Hz, 220 mJ/pulse, 50 Jcm^{-2}, 4.6 Wcm^{-2}, 25 pulses, 2 µs t_d, 4.5 µs t_i	External calibration with samples analyzed by a validated reference method	Drying, cryogenic grinding (95% of particles < 75µm) and pelletizing	20 (Si)	6
Leaves of sugar cane, soya, citrus, coffee, maize, bean, eucalyptus, mango, banana, grape, millet, rubber tree, tomato, and CRMs	Ca, Mg, P, Cu, Fe, Mn, Zn	Ti:Sapphire@800nm, 1 kHz, 1.65 mJ/pulse, 9.5 Jcm^{-2}, 1.6 x 10^5GW cm^{-2}, 30 pulses, 35 ns t_d, 250 ns; Nd:YAG laser @1064, 532 and 266 nm, 3.3 Hz, 70 mJ/pulse, 6 $GWcm^{-2}$, 35 Jcm^{-2}, 20 pulses, 35 µs t_d, 0.75 µs t_i	External univariate and multivariate (PLS) calibrations with samples analyzed by a validated reference method	Drying, cryogenic grinding, sieving (75µm pore diameter) and pelletizing	*fs-LIBS:* 7 (Ca), 20 (Mg), 400 (P), 7 (Cu), 12 (Fe), 2 (Mn), 80 (Zn); *ns-LIBS:* 5-10 (Ca), 10-50 (Mg), 100 (P), 1-3 (Cu), 3-8 (Fe), 1 (Mn), 4-14 (Zn)	25
Sugar cane	P, K, Ca, S, Fe,	Nd:YAG@1064nm, 10 Hz, 50 Jcm^{-2}, 48 pulses, 2 µs t_d, 5	External calibration with samples analyzed by a	Direct analysis of dried and flattened leaves	*n.r.*	17

leaves	Mn, Si	μs t_i	validated reference method			
Pasture vegetation	Na, K, Mg, Ca, Mn, Fe, Cu, Zn, B, P, S	Nd:YAG@1064 nm, 200 mJ/pulse, 8 pulses, 1 μs t_d	External multivariate (PLS) calibrations with samples analyzed by a validated reference method	Drying, grinding (< 1mm) and pelletizing	*n.r.*	89
Leaves and flowers of *Cannabis*	Al, Ba, Ca, Br, Cu, Fe, K, Mg, Mn, Na, P, Rb, Sr	Nd:YAG@1064 nm, 10 Hz, 200 mJ/pulse, 5.2 $GWcm^{-2}$, 2 pulses, 2 μs t_d	External calibration with CRMs	Drying (lyophilization), grinding and pelletizing	4.7 (Al), 0.22 (Ba), 69 (Ca), 0.1 (Br), 0.1 (Cu), 1.6 (Fe), 158 (K), 14.9 (Mg), 3.0 (Mn), 1.4 (Na), 22 (P), 0.1 (Rb), 0.8 (Sr)	108
Black tea leaves	Fe, Cr, K, Br, Cu, Si, Ca	Nd:YAG@266 nm, 20 Hz, 17.52 mJ/pulse, 317 and 357ns t_d	External calibration with samples analyzed by a validated reference method	Pelletizing	22 (Fe), 12 (Cr), 14 (K), 11 (Br), 6 (Cu), 1 (Si), 12 (Ca)	109
CRMs of plants	Al, Ca, Mg, Fe, K, Si	Nd:YAG@532 nm, 4 Hz, 20 mJ/pulse, 5.24 x 10^{12} Wcm^{-2} 20 pulses, 1.5 μs t_d	External multivariate calibration (PLS) with CRMs	Pelletizing	*n.r.*	90
Pasture	N, P, K, S, Ca, Mg, Fe, Mn, Zn, Cu, B, Na	Nd:YAG@1064 nm, 9 $GWcm^{-2}$, 1.27 μs t_d, 1 ms t_i	External multivariate calibration (PLS)	Direct analysis of fresh leaves and pelletizing	10^4 (N), $3x10^3$ (P), 10^4 (K), 10^3 (S), $2x10^3$ (Ca), 470 (Mg), 96 (Fe), 25 (Mn), 20 (Zn), 3 (Cu), 4 (B), 10^3 (Na)	106

n.r. = not reported.

Table 5 – Selected applications dealing with quantitative analysis of plant leaves by X-Ray Fluorescence Spectrometry

Matrix	Analytes	Technique	Calibration strategy	Sample preparation	LOD mg kg^{-1}	Ref
Orange and lemon leaves	Fe, Cu, Mn, Zn, Ti	EDXRF	Emission-transmission method	Analysis of fresh leaves and pellets after washing, drying and grinding	8 (Fe), 4 (Cu), 12 (Mn), 4 (Zn), 69 (Ti)	35
Higher plants, grasses, and mosses	P, K, Ca, Mg, S, Fe, Cu, Mn, Zn, Al, As, Cd, Co, Na, Pb, Sr	EDPXRF WDXRF	Fundamental parameters; spiked synthetic cellulose; IAEA-QXAS	Washing, drying, ball-milling and pelletizing	EDPXRF - from 1.1 (Pb) to 20 (Ca); WDXRF -from 0.5 (Co) to 400 (K); High energy EDPXRF - from 0.18 (Zn) to 0.7 (Cd)	112
Leaves and stem of *Portulaca oleracia* L.	K, Ca, Fe, Zn, Na	EDXRF	Emission-transmission method	Drying, grinding and sieving (20-mesh)	---	113
Leaves and roots of medicinal plants	K, Ca, Fe, Cu, Mn, Zn, Rb, Sr	EDXRF	Elemental sensitivities method	Washing, drying, grinding, sieving (<75 μm):. i) pressed powder; ii) water infusion; iii) solid residues	EDXRF: From 0.48 (Sr) to 400 (K); TXRF: from 0.32 (Sr) to 25.9 (K)	114
Medicinal plants	P, K, Ca, S, Fe, Cu, Mn, Zn, As, Br, Cl, Cr, Hg, Ni, Rb, Si, Sr, Ti, Zr	EDXRF	Elemental sensitivities method	Drying, grinding, sieving (< 75 μm) and pelletizing	---	115
Tomato leaves and fruits	N, P, K, Ca, Mg, S, Fe, Cu, Mn, Zn, Ba, Br, Cl, Mo, Rb, Si, Sr	EDPXRF	---	Drying, grinding, sieving (< 200 μm) and pelletizing	---	116
Rhizome, stalk, leaves and flowers of a medicinal plant	Fe, Cu, Mn, Zn, Ba, Cr, Ni, Sr, Ti	WDXRF	External calibration with CRMs	Drying, grinding (<100 μm) and pelletizing	1.5 (Fe), 0.4 (Cu), 0.8 (Mn), 0.4 (Zn), 4.0 (Ba), 2.6 (Cr), 0.3 (Ni), 1.7 (Sr), 3.4 (Ti)	117
Leaves of a medicinal herb	K, Ca, Fe, Cu, Mn, Zn, Cr, Co, Ni, Pb, Rb, Se, Sr, V	EDXRF	External calibration with CRMs	Drying, grinding and pelletizing	---	118
Leaves of bush cinquefoil and blue honeysuckle	K, Ca, Br, Cu, Fe, Mn, Nb, Ni, Rb, Sr, Ti, Y, Zn, Zr	SRXRF	External standard method	Drying, grinding and pelletizing	---	119

Corn and wheat plant tops, cotton leaves, and soybean grains	P, K, Ca, S, Fe, Mn, Zn, Co, Cr, Ni, Si	P-XRF	External calibration with samples analyzed by a validated reference method	Loose powder (Mylar® thin film)	---	111
Grass, wheat and *Deschampsia caespitosa* (L.)	Si, P	P-XRF	External calibration with methyl cellulose spiked with Si and P, and CRMs	Drying, ball-milling and pelletizing	140 (Si), 130 (P)	9
Leaves and stalks of *Catha edulis*	P, K, Ca, Mg, S, Fe, Cu, Mn, Zn, Al, Br, Cl, Na, Ni, Rb, Si, Sr, Ti	WDXRF	Fundamental parameters	Drying, grinding, sieving (< 32 µm) and pelletizing	---	96
Sugar cane leaves	P, K, Ca, S, Fe, Mn, Si	µ-EDXRF	External calibration with samples analyzed by a validated reference method	Drying, grinding and pelletizing	From 29 (Mn) to 2271 (Si)	8
Coffee leaves and branches	P, K, Ca, Mg, Cu, Fe, Zn, Mn, Ni	EDXRF	External calibration with samples analyzed by a validated reference method	Drying, ball-milling, sieving (< 500 µm). Loose powder (Mylar® film)	From 2.1 (Zn) to 547 (Mg)	78
Sugar cane leaves	P, K, Ca, S, Fe, Mn, Si	Portable and benchtop EDXRF	External calibration with samples analyzed by a validated reference method	Drying, grinding and pelletizing	20 (Fe, Mn), *ca.* 100 (P, K, Ca, S) and 200 (Si) – benchtop; 250 (P) and 500 (Si) - Portable	22
Pepper leaves and fruits	P, K, Ca, Mg, S, Fe, Cu, Mn, Zn, Al, Ba, Br, Ce, Cl, La, Mo, Ni, Rb, Si, Sr	EDPXRF	---	Drying, grinding (<200 µm) and pelletizing	---	120
Sugar cane leaves	P, K, Ca, S, Fe, Mn, Si	EDXRF	External calibration with samples analyzed by a validated reference method	Direct analysis of dried and flattened leaves	---	17
Aquatic plants	P, K, Ca, Mg, S, Fe, Cu, Mn, Al, Cl, Cr, Ni, Pb, Si, Sr, Ti	WDXRF	External calibration with CRMs and synthetic standards	Drying, grinding (<100 µm) and pelletizing	---	71
Seeds and leaves of cowpea, croton, pulp and leaves of mango, saw dust of cyprus and mahogany, leaves and stem of maize, leaves and bark of prunus	Na, Mg, Al, P, S, K, Ca, Mn, Fe	P-XRF	External calibration with samples analyzed by a validated reference method	Drying, grinding. Loose powder with or without Prolene® thin film	---	110
Fresh corn leaves	P	P-XRF (*in situ*)	Linear correlations between P Kα emission line intensities (normalized by	Direct XRF scans were performed on the first uppermost true leaf	---	121

			the Ag Lα scattered line) and the elemental mass fractions			
Fresh sugar cane leaves	K, Ca, S, Si	P-XRF (*in situ*)	Averaged emission line intensities from all leaf fragments were correlated with the comparative mass fractions values	Leaf fragments were cleaned with deionized water and superficially dried with a paper towel	K (0.48), Ca (0.24), S (0.51), and Si (0.35)	123

Table 6 – Chemical imaging of plant tissues employing micro-X-Ray Fluorescence Spectrometry with Synchrotron radiation source

Matrix	Analytes	Spot size (µm)	Sample preparation	Objective	Imaging	Ref
Leaves of a Cd-hyperaccumulating plant	Ca, Mn, Zn, Cd	3.8 x 1.3	Cutting, flattening, and covering with a Mylar® film	Investigation of the Cd accumulation mechanism	Qualitative	129
Leaves of a peach-almond hybrid plant	Ca, K, Cl, S, Fe, Mn, Zn, Cu	100	Washing, drying on absorbent paper, and analysis of leaf pieces (3 x 3 mm)	Investigation of the effects of Fe re-supply on the changes in Fe and chlorophyll concentrations and nutrient distribution	Qualitative	130
Roots, stems, and leaves and flowers of sunflower	[a] Pb, Zn	200	Washing, pressing between papers, and drying	Evaluation of a benchtop EDXRF instrument in phytoremediation and plant biology studies	Quantitative	131
Leaves of tomato plants	Fe, K, Ca, Cu, Ni, Zn, Br, Mn	20	Leaf tissues: washing and freezing in liquid N_2; freeze-drying under vacuum and selection of an area of 2 mm^2 to analyze.	Investigation of the contribution of different natural chelates to Fe-acquisition, evaluating the micronutrient fraction allocated at the leaf level.	Qualitative	132
Leaves and stems of a Zn/Cd cohyperaccumulator and Pb accumulator plant	P, K, Ca, S, Zn, Pb	3.5 x 5.5	Cutting, thin sections preparation with a cryomicrotome	Investigation of the spatial distribution and speciation of Pb in an accumulator plant	Qualitative	133
Roots of cowpea	Cu, Zn, Ni	2 x 2	Root sections were placed between two pieces of Kapton® polyimide	Evaluation of the *in situ* distribution	Qualitative	134

			film to minimize dehydration	and speciation of Cu, Ni, and Zn in roots of a non-hyperaccumulator		
Roots and rice grains	Ca, K, Fe, Mn, Zn, As	5 and 15	Roots: cutting and drying. Grains: removal of the husks and thin-sections preparation	Characterization of the mineral phases of Fe coatings on rice roots and quantification of plant nutrients and As species in roots and grains	Quantitative	135
Roots, leaves, and trichomes of cucumber	K, Ca, Ti	0.33 × 0.65	Roots and leaves: cleaning, cutting, freezing, embedment in resin, cutting in thin-sections, and mounting onto Ultralene® film	Evaluation of the spatial distribution and speciation of TiO_2	Qualitative	136
Roots, nodules, stems, and pods of soybean	K, Ca, Zn, Ce	0.6 x 1.1 and 2 x 2	Washing, cutting, embedment into resin, cutting with a cryomicrotome, mounting onto Kapton® and Ultralene®, freeze-drying	Evaluation of the forms of Ce and Zn within soybean tissues previously treated with ZnO and CeO_2 nanoparticles	Qualitative	137
Root tips of cucumber	Cu, Fe, Mn, Ca, K	3 x 3	Root tips and root hairs were cut and fixed on a 3M® tape in liquid nitrogen. Samples were freeze-dried.	Investigation of the spatial distribution and speciation of Cu.	Qualitative	138
Roots of wheat and rice	As	---	Roots were cut and placed between two pieces of 8 µm-thick Kapton® polyimide film to minimize dehydration	Evaluation of *in situ* accumulation and transformation of As within root tissues	Qualitative	139
Roots and leaves of cucumber	Ce, La	5 x 7	Washing, immersion in embedding medium, freezing, cutting with a cryomicrotome, fixing onto 3 µm thick Mylar® film,	Phytotoxicity evaluation of CeO_2 and La_2O_3 nanoparticles	Qualitative	140

			drying			
Three fractions of rice grain (hull, bran, and white rice)	K, Ca, Fe, Cu, Mn, Zn, Cd, Hg, Se	50 (diameter)	Rinsing in the field with drinking water, cleaning with deionized water in an ultrasonic bath, and drying. Cutting, mounting onto a plastic support, slicing with a cryomicrotome. The 150µm thick sections were placed on Kapton® tape	Investigation of the speciation and localization of Hg	Qualitative	141
Pinnae, stipes and roots of ferns	[a] As, P	50	Fixing with adhesive tape onto a 4µm Mylar® film.	Evaluation of the As and P microchemical mapping in plants grown in the absence and in As enriched solutions.	Qualitative	79
Nodes and internodes of rice plants	As	5 µm for node and 2 µm for internode	Cutting, placing in MES buffer, cutting, placing into a planchette coated with hexadecane and another planchette was placed on top. Sections were frozen, embedded in resin and sectioned.	Investigation of the role of rice nodes in As storage and distribution.	Quantitative	142
Roots of maize and sunflower, and topsoil	As, K, Ca, Si, Fe	2 × 5	Drying, embedment into epoxy casting resin under vacuum, slicing after drying with a diamond saw and polishing. The 100 µm-thick sections were transferred to Mylar® film.	Investigation of the accumulation of arsenic (As) in and on roots	Quantitative	143
Leaf petioles of sunflower	Zn, Ca, K	2	Mid-sections of leaf petioles were cut. The 100 µm-thick leaf cross-sections were cut with a cryotome and freeze-dried prior to analysis.	Evaluation of elemental distribution and transport following the application of various Zn formulations.	Qualitative	144

Leaves of cucumber plants	Fe	20	Washing, drying with filter paper and flattening between two plastic disks. Immersion in liquid nitrogen and then freeze-dried under vacuum. The intact flat freeze-dried leaves were taped on a hollow aluminum sample holder.	Investigation of the dynamics of Fe accumulation and distribution within leaf tissues of Fe-deficient cucumber plants.	Quantitative	145
Kernels and leaves of corn	Ca, Fe, Cu, K, Mn, Zn	---	Washing, transversally cutting, freezing, fixing with Tissue Tek® and sectioned with a cryomicrotome. The 30 µm-thick sections were mounted onto Kapton® tape and freeze-dried.	Investigation of interaction of NPs of CeO_2 and ZnO with corn through the life cycle of the plant.	Qualitative	146
Transversal and longitudinal sections of carrots	[a] P, S, K, Br	25	Washing, cutting into 0.2 mm tangential and longitudinal sections using stainless steel surgical blade, ultra-freezing and lyophilization. Sections were placed on a plastic support.	Evaluation of the analytical capabilities of two benchtop XRF systems (EDXRF and µ-XRF) for multielemental analysis and imaging of vegetal foodstuffs.	Qualitative	147
Wheat grains	[a] P, K, Ca, Cl, Cu, Zn, Fe, S, Mn	25	Cutting and gluing onto a Mylar foil.	Evaluation of benchtop µ-XRF capabilities for mapping and its potentialities to differentiate element distribution in biofortified and control wheat grains.	Qualitative	148
Roots of rice	Cu	20	Fresh roots: cutting and rinsing with deionized water. Root tips and maturation zone of fresh roots: cutting, freezing and freeze-dried. The 40 µm-thick root sections were cut with a cryotome and then freeze-dried.	Investigation of the *in vivo* characteristics of Cu distribution patterns and its speciation model.	Quantitative	149

Tomato plants (roots, stems, leaves and fruits)	[a] K, Ca, Fe, S, Sr, Br, Cl, Zn, Mn, Cu.	250 µm and 650µm for the micro measurements	Cleaning up using water. Roots and stems: prepared as cross-sections; tomato fruit: cutting in two halves, cross-sectioned and preparing thin slices; leaves: no preparation. All samples: flattening and drying.	Investigation of the distribution of several elements in roots, stems, leaves and fruits of *Solanum lycopersicum* plant.	Qualitative	150

[a] Benchtop micro-X-ray fluorescence spectrometry.

FIGURES

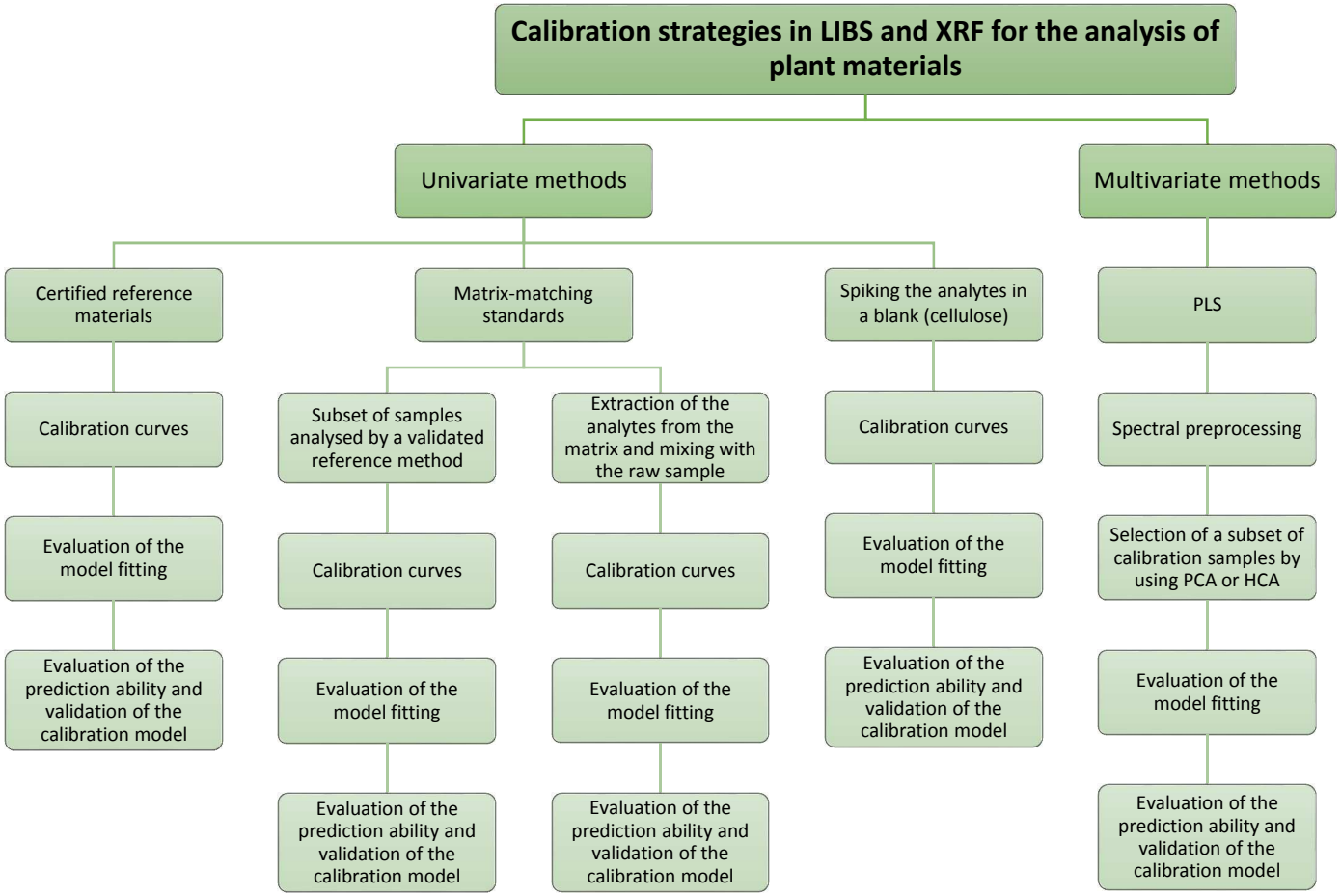

Figure 1 – Calibration strategies in LIBS and XRF analysis of plant materials.

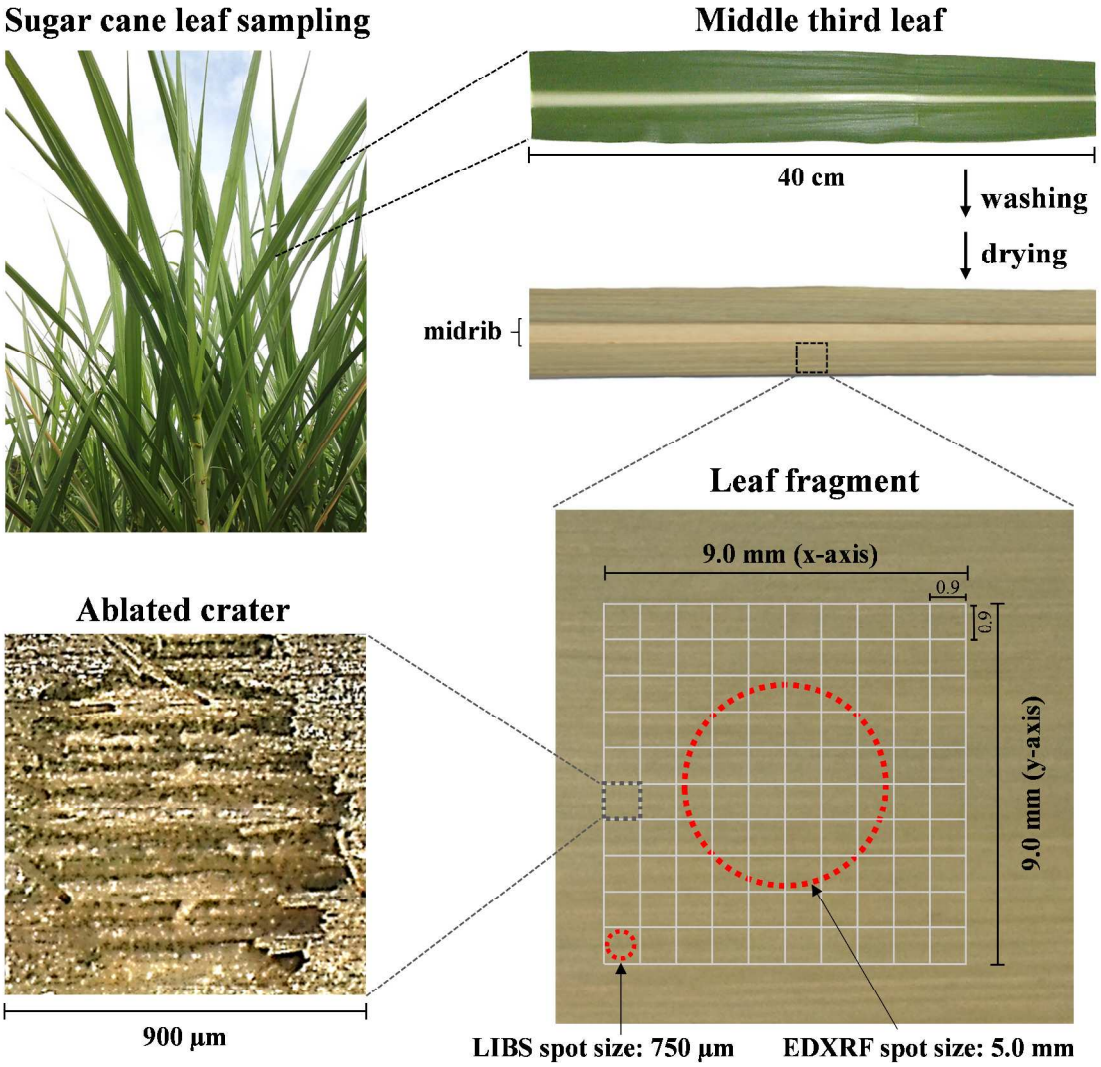

Figure 2 - Schematic overview of the sampling protocol for LIBS and EDXRF direct analysis of sugar cane leaves. Leaf fragment depicts a 9 mm x 9 mm sampling grid (n = 100 sampling spots) used in the chemical mapping, as well as EDXRF and LIBS spot sizes. Ablation craters obtained after analysis with LIBS by applying 5 consecutive laser pulses (50 J cm^{-2}, 10 Hz, 1064 nm) *per* site. Reproduced from Ref. [17] with permission from The Royal Society of Chemistry.

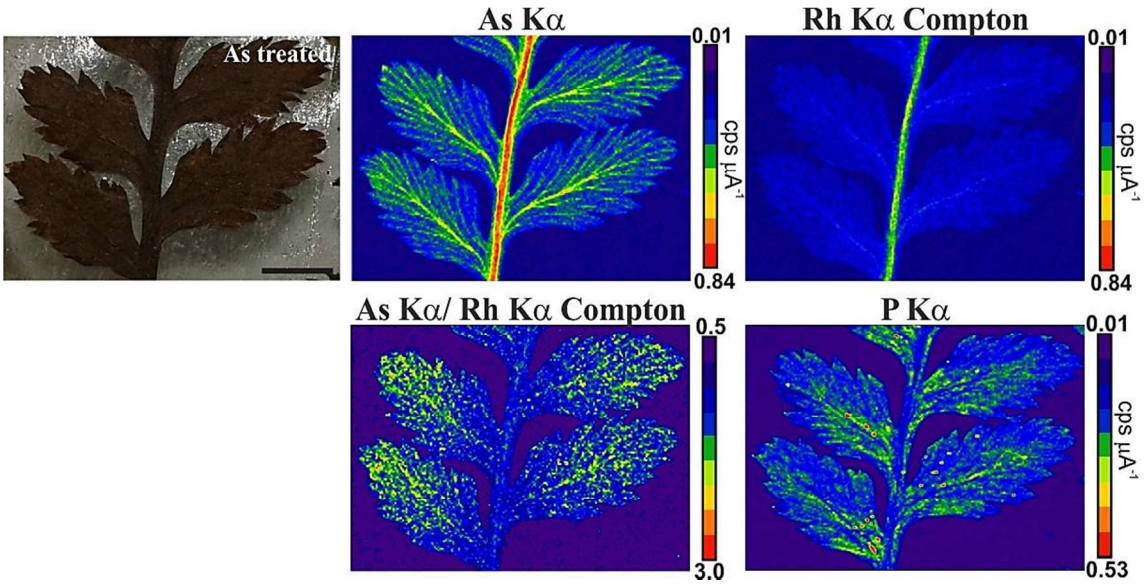

Figure 3 – Microchemical maps obtained by μ-XRF for As and P in the pinnules of *Pityrogramma calomelanos* hydroponically grown with 30 x 10^{-3} mol L^{-1} As. The Rh Kα Compton peak was used for correcting the As maps. Reproduced from Campos et al.[79] with permission from The Royal Society of Chemistry.

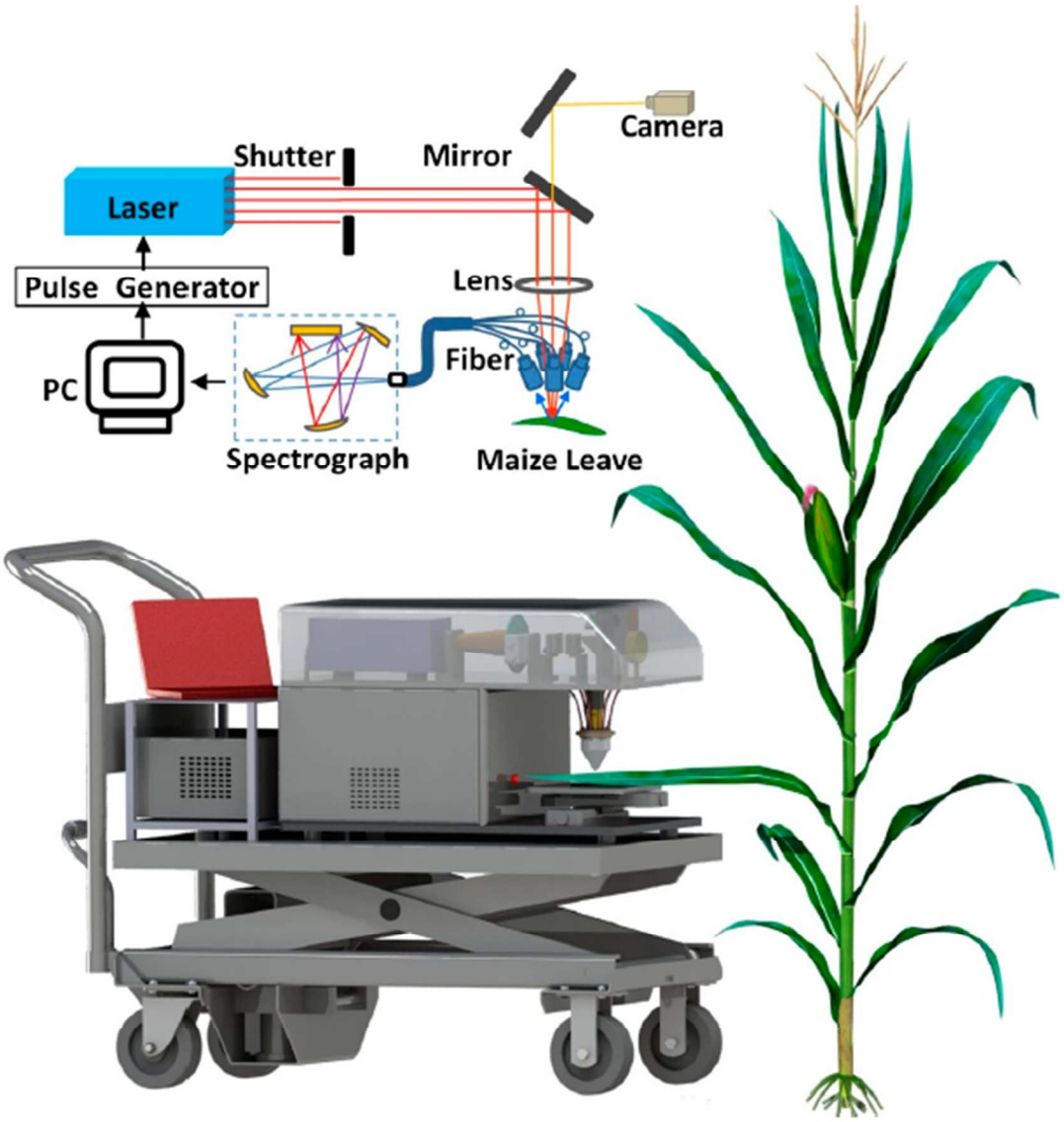

Figure 4 – Schematic overview of the LIBS system applied for the *in situ* and *in vivo* elemental mapping of maize leaves previously sprayed with an organophosphorus pesticide (chlorpyrifos, $C_9H_{11}Cl_3NO_3PS$). Reproduced from Zhao et al.,[198] with permission from MDPI Open Access Journals.